

Supporting Information for

Coherent Light Harvesting through Strong Coupling to Confined Light

Gerrit Groenhof^{1*} J. Jussi Toppari²

¹Department of Chemistry and Nanoscience Center, P. O. Box 35, FIN-40014 University of Jyväskylä, Finland

²Department of Physics and Nanoscience Center, P. O. Box 35, FIN-40014 University of Jyväskylä, Finland.

Contents:

Multi-scale simulation model	2
Force field parameters	6
Molecular dynamics simulation setups	6
Spectra	8
Results & Discussion	8
Figures S1-S30	12
Animations	42
References	42

Multi-scale simulation model

Our multi-scale model for simulating molecules strongly coupled to confined light modes is described in detail by Luk *et al.*¹ and we refer the interested reader to that article. Here we only give a brief outline of the main ideas.

Our approach is a hybrid quantum mechanics / molecular mechanics (QM/MM) extension of the Jaynes-Cummings model for strong light-matter interactions.² The Jaynes-Cummings model was originally derived for a two-level system (atom) coupled to confined light modes:

$$\hat{H}_{\text{JC}} = \hbar\omega_a\hat{\sigma}^\dagger\hat{\sigma} + \hbar\omega_{\text{cav}}\hat{a}^\dagger\hat{a} + \hbar g(\hat{a}^\dagger\hat{\sigma} + \hat{a}\hat{\sigma}^\dagger) \quad (1)$$

Here $\hbar\omega_a$ is the excitation energy of the two-level atom and $\hbar\omega_{\text{cav}}$ is the energy of the cavity photon. The operator $\hat{\sigma}^\dagger$ ($\hat{\sigma}$) creates (annihilates) the excitation of the atom, while \hat{a}^\dagger (\hat{a}) creates (annihilates) a photon in the cavity. The strength of the light-matter interaction, $\hbar g$, is calculated within the dipole approximation as the overlap between the transition dipole moment ($\boldsymbol{\mu}$) for the excitation of the atom and the vacuum field of the confined light mode:

$$\hbar g = \boldsymbol{\mu} \cdot \mathbf{u}_{\text{cav}} \sqrt{\hbar\omega_{\text{cav}}/\epsilon_0 V_{\text{cav}}} \quad (2)$$

Here, V_{cav} is the effective mode volume of the cavity, ϵ_0 the vacuum permittivity and \mathbf{u}_{cav} the unit vector indicating the direction of the electric component of the confined mode.

Within the single-excitation subspace (*i.e.*, a single photon in the cavity or atom), the solutions to the Jaynes-Cummings Hamiltonian are coherent super-positions of the electronic excitation in the atom and of the excitation in the cavity (*i.e.*, presence of a photon). Tavis and Cummings extended this model to many atoms and the eigenstates in the single excitation subspace are now super-positions of all uncoupled states in which either a single atom is excited, or a single photon is in the cavity.³

The Jaynes-Cummings² and Tavis-Cummings³ models are valid for two-level emitters in cavities but cannot predict nor rationalize the effect of strong coupling on the dynamics of molecular systems with very many degrees of freedom. Following Galego, Feist and Garcia-Vidal,⁴ we have extended the zero-dimensional Jaynes-Cummings model to a fully atomistic method that describes the high-dimensional molecular energy landscape, including the effects of environment, temperature and pressure.¹

The key assumption in our model is that the electrons and cavity photon adapt instantaneously to displacements of the nuclei. We therefore separate the nuclear degrees of freedom from the much faster electronic plus photonic degrees of freedom.⁴ As a consequence, the energy levels of the Tavis-Cummings Hamiltonian are now functions of the nuclear coordinates ($\mathbf{R}(t)$) of N molecules and form the hybrid light-matter (*i.e.*, polaritonic) potential energy surfaces on which the nuclei move.¹

For N molecules with M atoms per molecule, the Tavis-Cummings Hamiltonian is a $N + 1$ by $N + 1$ matrix:

$$\mathbf{H} = \begin{pmatrix} H_{1,1} & 0 & \cdots & 0 & H_{N+1,1} \\ 0 & H_{2,2} & \cdots & 0 & H_{N+1,2} \\ \vdots & \vdots & \ddots & \vdots & \vdots \\ 0 & 0 & \cdots & H_{N,N} & H_{N+1,N} \\ H_{1,N+1} & H_{2,N+1} & \cdots & H_{N,N+1} & H_{N+1,N+1} \end{pmatrix} \quad (3)$$

where the elements are functions of the $3M$ atomic coordinates of all (N) molecules (plus environment) and are computed at the QM/MM level.¹

The diagonal elements are the usual 'bare' (*i.e.*, outside cavity) electronic QM/MM energies of the ground (S_0) or excited states (S_1). The first N diagonal elements represent the cases in which one (i) of the N molecules is excited, while the other molecules are in the ground state. The element $H_{N+1,N+1}$ models the situation in which all molecules are in the electronic ground state, while there is a single photon with energy $\hbar\omega_{\text{cav}}$ in the cavity.

The off-diagonal elements describe the interactions between the molecules and the cavity photon and are approximated as the overlap between the QM/MM transition dipole moment and the electric field of the confined cavity photon (equation 2), as in the Jaynes-Cummings model.² The matrix is diagonalized at every time step of the molecular dynamics (MD) simulation to yield the $N + 1$ hybrid light-matter polaritonic states:

$$\psi_K = \sum_{i=1}^N \beta_i^K |g_1 g_2 \dots e_i \dots g_N\rangle |0\rangle + \alpha^K |g_1 g_2 \dots g_i \dots g_N\rangle |1\rangle \quad (4)$$

where $|g_i\rangle$ and $|e_i\rangle$ are the ground and excited states of molecule i , while $|1\rangle$ or $|0\rangle$ indicate whether there is a *single* photon in the cavity or not. The β_i^K and α^K are expansion coefficients and the index K labels the $N + 1$ eigenstates of the system.

Our model is valid within the *single* photon manifold of the strong coupling regime. In the regimes of ultra-strong and deep strong coupling, where the coupling strengths become comparable to the transition frequencies, additional self-interaction terms must be included,⁵⁻⁷ which are neglected here.

Trajectories of M atoms in each of the N molecules are computed by numerically integrating Newton's equations of motion associated with the QM/MM potential energy surface of one of these states:

$$V_K(\{\mathbf{R}_1, \mathbf{R}_2, \dots, \mathbf{R}_M\}_1, \{\mathbf{R}_1, \mathbf{R}_2, \dots, \mathbf{R}_M\}_2, \dots, \{\mathbf{R}_1, \mathbf{R}_2, \dots, \mathbf{R}_M\}_N) \quad (5)$$

with $\{\mathbf{R}_1, \mathbf{R}_2, \dots, \mathbf{R}_M\}_i$ the Cartesian coordinate vectors of the M atoms in molecule i . The forces acting on the atoms of all molecules are computed with the Hellmann-Feynman theorem.

The classical trajectories always move on *single* polaritonic potential energy surface (V_K), but transitions between surfaces are possible. Two approaches were used in this work to model such transitions: (i) *adiabatic* hopping,⁸ and (ii) Tully's fewest switches surface hopping.⁹

Diabatic hopping

The *diabatic* surface hopping algorithm is based on the Landau-Zener model,^{10,11} which relates the probability of a transition between two states ψ_K and ψ_J to the *non-adiabatic* coupling, via:

$$P_{K \rightarrow J} = \exp\left(-\frac{1}{4}\pi\xi\right) \quad (6)$$

with ξ the Massey parameter, defined as:¹²

$$\xi = \frac{\Delta E_{KJ}}{\hbar \left\langle \psi_K \left| \frac{\partial}{\partial t} \right| \psi_J \right\rangle} \quad (7)$$

Following Hammes-Schiffer and Tully,¹³ we approximate the *non-adiabatic* coupling $\left\langle \psi_K \left| \frac{\partial}{\partial t} \right| \psi_J \right\rangle$ as $\langle \psi_K(t) | \psi_J(t + \Delta t) \rangle / \Delta t$, *i.e.*, the overlap between the state ψ_J at the current time step and the state ψ_K at the previous time step. Under the additional assumption that the uncoupled molecular wave functions vary slowly, we can further approximate this overlap as the inner product of the eigenvectors of the Tavis-Cummings matrix (equation 4):

$$\langle \psi_K(t) | \psi_J(t + \Delta t) \rangle = \sum_i^N \beta_i^K(t) \beta_i^J(t + \Delta t) + \alpha^K(t) \alpha^J(t + \Delta t) \quad (8)$$

Calculating this overlap and the energy gap ΔE_{KJ} at every time step is straightforward and we can use the Landau-Zener formula to calculate the probability of a transition to the other surface (equation 6). In principle, this transition probability could be used to spawn a new trajectory on the other polaritonic surface, but since this procedure would lead to multiple trajectories that have to be computed simultaneously, spawning will be too demanding in practice. Instead, we restricted hopping to situations where the transition probability approaches unity. This happens when the states K and J are degenerate: $\Delta E_{KJ} \approx 0$ and $\langle \psi_K(t) | \psi_J(t + \Delta t) \rangle > \langle \psi_K(t) | \psi_K(t + \Delta t) \rangle$. However, because the very strict *diabatic* hopping criterion can lead to an underestimation of the population transfer probability,¹⁴ we also performed the simulations with the more sophisticated Fewest Switches Surface Hopping method.⁹

Tully's Fewest Switches Surface Hopping

The total *time-dependent* light-matter wave function is expanded in the basis of the $N + 1$ polaritons, *i.e.* the eigenvectors of the Tavis-Cummings Hamiltonian matrix (equation 4), at the current coordinates of the M atoms in each of the N molecules:

$$\Psi(t) = \sum_K^{N+1} c_K(t) \psi_K \quad (9)$$

and evolved along the trajectory of the N molecules with the exponential unitary propagator (UP):

$$\mathbf{c}(t) = e^{-i\mathbf{H}_p(t+\frac{1}{2}\Delta t)\Delta t} \cdot \mathbf{c}(t + \Delta t) \quad (10)$$

Here $\mathbf{c}(t)$ is the vector of the time-dependent expansion coefficients $c_K(t)$ in equation 9, Δt is the time step with which the classical trajectories are propagated and \mathbf{H}_p is the light-matter Hamiltonian, including the *non-adiabatic* couplings between the polaritons:

$$(\mathbf{H}_p)_{KJ}(t + \frac{1}{2}\Delta t) = \frac{V_K(t) + V_K(t + \Delta t)}{2\hbar} \delta_{KJ} - \frac{i}{2\Delta t} [\langle \psi_K(t) | \psi_J(t + \Delta t) \rangle - \langle \psi_K(t + \Delta t) | \psi_J(t) \rangle] \quad (11)$$

where δ_{KJ} is the Kronecker delta and the term between square brackets approximates the non-adiabatic coupling between polaritons ψ_K and ψ_J .¹³ As in *diabatic* hopping, we compute these overlaps as the inner product of the eigenvectors of the Tavis-Cummings Hamiltonian (equation 8).

Hops between polaritonic surfaces occur when the probability of a transition from the current state K to another state J is larger than a random number ζ on the interval from 0 to 1. In Tully's Fewest Switches Surface Hopping (FSSH), the total number of hops is minimized if the probability of a hop from K to J is computed as:⁹

$$\sum_L^J P_{KL} < \zeta < \sum_L^{J+1} P_{KL} \quad (12)$$

with

$$P_{KL} = \max \left[\frac{2 \operatorname{Re} \left(c_K^* c_L (\mathbf{H}_p)_{KL} (t + \frac{1}{2}\Delta t) \right) \Delta t}{c_K^* c_K} \right] \quad (13)$$

In contrast to more recent implementations of the FSSH, we did not apply an *ad hoc* decoherence correction. We consider this reasonable for large ensembles with hundreds of molecules, because the polaritonic states, which mainly differ in the excitation of a single molecule, are almost parallel. Therefore, the forces acting on the molecules in various states will be very similar and thus largely cancel the effects of decoherence, which would be strongest if the potential energy surfaces are very different. Furthermore, we observed that as soon as the excitation is localized on a single reactive molecule, there are no transitions back due to a steeply increasing energy gap.

The eigenvectors (ψ_K) are only determined up to their phase (sign) and the eigenvectors can switch sign during the simulation. Because this could lead to artificially small couplings in equation 11, we corrected sign changes by tracking the eigenvectors between subsequent time-steps and equating their signs. The state tracking was also used to automatically identify un-avoided crossings, which can occur when coupling is weak, or absent.¹⁵ Un-avoided crossings were enforced if the overlap between two states exceeds a threshold of 0.9.

The multi-scale polaritonic molecular dynamics model,¹ including the fewest switches surface hopping algorithm, was implemented in Gromacs, version 4.5.¹⁶ Because the excited and ground state energies and transition dipole moments can be computed for each molecule on a separate node of a computer-cluster, while communication is limited to only $3N$ double precision numbers per MD step,¹ the code scales optimally until the two matrix diagonalization steps (equations 3 and 11) become rate limiting.

Force field parameters

For the Rhodamine model (Rho) we used the Amber03 force field¹⁷ described in Luk *et al.*,¹ while for 2-(2'-hydroxyphenyl)benzothiazole (HBT) the Gromos-2016H66 parameter set was used.¹⁸ Because in our simulations HBT and Rho only interact via the cavity photon, there are neither Coulomb nor Van der Waals interactions between the two molecules. Therefore, describing the two molecules with different force fields in our simulations cannot introduce artifacts associated with mixing incompatible interaction models.

The Gromos-2016H66 force field was chosen for HBT because it contains a validated cyclohexane model,¹⁸ which was used as the solvent for HBT in our simulations. In this united atom representation of cyclohexane, none of the atoms carries a partial charge. Because HBT was kept frozen during the solvent equilibration and modeled at the QM level in all other simulations, there was no need to assign partial charges to the HBT atoms. The Gromos atom-types used in the simulations are listed in Figure S1.

Molecular dynamics simulation setups

Rhodamine

The Rhodamine model, shown in Figure S2, was placed at the center of a rectangular box filled with 3,684 TIP3P water molecules.¹⁹ The simulation box thus contained 11,089 atoms and was equilibrated for 2 ns with harmonic restraints on the heavy atoms of the Rhodamine molecule (force constant $1000 \text{ kJmol}^{-1}\text{nm}^{-2}$). Subsequently, a 200 ns classical molecular dynamics (MD) trajectory was computed at constant temperature (300 K) using a stochastic dynamics integrator with a friction coefficient of 0.1 ps^{-1} . The pressure was kept constant at 1 bar using the Berendsen isotropic pressure coupling algorithm²⁰ with a time constant of 1 ps. The LINCS algorithm was used to constrain bond lengths,²¹ while SETTLE was applied to constrain the internal degrees of freedom of the water molecules,²² enabling a time step of 2 fs in the classical MD simulations. A 1.0 nm cut-off was used for Van der Waals' interactions, which were modeled with Lennard-Jones potentials. Coulomb interactions were computed with the smooth particle mesh Ewald method,²³ using a 1.0 nm real space cut-off and a grid spacing of 0.12 nm. The relative tolerance at the real space cut-off was set to 10^{-5} .

From the second half of the 200 ns MD trajectory 1,000 snapshots were extracted at 100 ps intervals and subjected to a further equilibration of 10 ps at the QM/MM level. The time step was reduced to 1 fs. As in previous work,¹ the fused ring system was included in the QM region, described at the RHF/3-21G, while the rest of the molecule as well as the solvent were modelled with the Amber03 force field.¹⁷ The bond connecting the QM and MM subsystems was replaced by a constraint and the QM part was capped with a hydrogen atom. The force on the cap atom was distributed over the two atoms of the bond. The QM system experienced the Coulomb field of all MM atoms within a 1.6 nm cut-off sphere and Lennard-Jones interactions between MM and QM atoms were added. The singlet electronic excited state (S_1) was modeled with the Configuration Interaction method, truncated at single electron excitations, for the QM region (*i.e.*, CIS/3-21G//Amber03).

Hydroxyphenyl-benzothiazole (HBT)

HBT (Figure S1) was placed at the center of a rectangular box that was filled with 460 cyclohexane molecules. The simulation box, which thus contained 2,785 atoms, was equilibrated for 100 ns. During equilibration, the coordinates of the HBT atoms were kept fixed. The LINCS algorithm was used to constrain bond lengths in cyclohexane,²¹ enabling a time step of 2 fs. Temperature and pressure were maintained at 300 K and 1 atmosphere by means of weak-coupling to an external bath ($\tau_T = 0.1$ ps, $\tau_P = 1$ ps).²⁰ The Lennard-Jones potential was truncated at 1.4 nm.

Snapshots were extracted from the equilibration trajectory and further equilibrated at the QM/MM level with a time step of 1 fs. HBT was modelled with density functional theory (DFT), using the CAM-B3LYP functional²⁴⁻²⁷ in combination with a 6-31G(d) basis set.²⁵ The cyclohexane solvent was described with the 2016H66 parameter set of the Gromos force field.¹⁸ The QM subsystem was mechanically embedded and because cyclohexane atoms are uncharged, the interactions between the QM and MM regions were modeled with Lennard-Jones potentials only. We used time-dependent density functional theory²⁸ to model the singlet excited electronic state of HBT in our simulations. The TD-CAM-B3LYP/6-31G(d)//Gromos-2016H66 model for photo-excited HBT in cyclohexane was validated by performing also excited-state MD simulations outside of the cavity and comparing the results to previous simulations^{29,30} and experiments.³¹

Cavity systems

In this work, we assume a cavity with an infinitely high quality-factor (Q-factor), *i.e.*, an infinite photon lifetime. Therefore, we modeled the cavity spectrum as a delta function, centered at the cavity frequency (ω_{cav}). Although not done in this work, a finite cavity Q-factor can be included as well via stochastic jumps to the ground state.¹ The probability for such jumps are determined by the cavity Q-factor, which is thus a parameter in the simulation, and the weight of the cavity photon in the hybrid state. The energy of the cavity photon ($\hbar\omega_{\text{cav}}$) was tuned at the excitation maximum of a single Rhodamine molecule in water, evaluated at the QM/MM level (4.15 eV).¹ The cavity volumes were chosen to yield Rabi splittings of up ~ 0.5 eV, irrespective of the number of molecules in the cavity. A Rabi splitting of several hundreds of meV is in line with experiments.³²⁻³⁵ The molecules were oriented to maximize the overlap of the transition dipole moment with the direction of the electric component of the confined light mode at the start of the simulations. Because we assume that HBT and Rhodamine are present in two separate layers, choosing the maximum overlap implies that we always couple to the *second* mode of the cavity, whose electric field maxima coincide with the centers of the molecule layers (Figure 1a, main text).

Because the molecules only interact via the cavity photon, there are no issues in using different QM/MM descriptions for the two molecules. Although the solvents as well as the force fields and QM methods were chosen because of convenience, we emphasize that for the purpose of this work it is not essential to have the most accurate description of the bare excitation energies of the molecules, but rather to have a realistic model of the molecular degrees of freedom, including the solvent environment. Including an explicit solvent environment goes significantly beyond the neglect or implicit treatment of the environment in phenomenological models of strong coupling, such as the

Lindblad formalism.³⁶ In all simulations a time step of 1 fs was used. All simulations were performed with the QM/MM interface between Gromacs-4.5¹⁶ and Gaussian09.³⁷

Spectra

Excitation spectra of the *single* molecules were computed from QM/MM trajectories in the ground (S_0) state. These spectra were composed of the S_1 - S_0 energy gaps (between 100 and 1,000 snapshots) by super-position of Gaussian functions:

$$I(E) = \sum_i^M \frac{2m_e}{3\hbar^2} \Delta E_i e^{-(E-\Delta E_i)^2/2\sigma^2} \mu_i^2 \quad (14)$$

where I is the intensity as a function of excitation energy (E), m_e the electron mass, M number of snapshots included in the analysis, ΔE_i the excitation energy in snapshot i and μ_i the transition dipole moment of that excitation. A width of $\sigma = 0.025$ eV was chosen for the convolution.

The one-photon excitation spectrum of an *ensemble* of molecules inside a cavity (Figure 1c) was computed in the same way, but using the oscillator strength of an ensemble of N molecules strongly coupled to confined light:

$$I(E) = \frac{2m_e}{3\hbar^2} \sum_i^M \left[\sum_{K=1}^{N+1} \left[(E_i^K - E_i^0) e^{-[E-(E_i^K - E_i^0)]^2/2\sigma^2} \sum_k^N \beta_{ki}^K \mu_{ki}^2 \right] \right] \quad (15)$$

where M is the number of snapshots of an ensemble of N molecules (plus environment) coupled to a confined light mode; E_i^K is the energy of polariton K in snapshot i , and E_i^0 is the ground state energy of $|g_1 g_2 \dots g_k \dots g_N\rangle$; β_{ki}^K is the expansion coefficient of $|g_1 g_2 \dots e_k \dots g_N\rangle$ in polaritonic state K (*i.e.*, the k^{th} molecule excited, others in the ground state, equation 4) in the i^{th} snapshot and the sum over k includes all N molecules. As for the molecules outside of the cavity, a width of $\sigma = 0.025$ eV was used to convolute the cavity spectra.

Results & Discussion

QM/MM spectra of Rhodamine and HBT

Figure S3 shows the absorption spectrum of Rho and of HBT. The spectra of both molecules are blue-shifted with respect to experiment due to limitations in the simulation models. The accuracy of the Rhodamine model likely suffers from (i) the QM/MM subdivision within the molecule, (ii) the rather small basis set and (iii) the truncated Configuration Interaction scheme. For HBT, the overestimation of the excitation energy at the TD-CAM-B3LYP/6-31G(d) (4.05 eV) with respect to experiment (3.68 eV)³¹ is in line with previous molecular dynamics studies at the TD-B3LYP/SV(P) level (3.86 eV)²⁹ or FOMO-CASSCI/6-31G(d) (6.07 eV).³⁰ Nevertheless, the overestimation of the excitation energy is not relevant for exploring the principles of polariton assisted energy transfer in this study. Furthermore, our model contains the molecular degrees of freedom, including those of the environment, which, in contrast to perfect agreement of the excitation energy, are essential to obtain an unbiased description of the energy transfer and reactivity under strong coupling. In

future work, however, we will aim for more realistic model systems in order to aid experimental validation of the concept.

Simulations of HBT in cyclohexane

Figure S4 shows the distance between the oxygen and hydrogen atom in 17 excited state molecular dynamics simulations of HBT in cyclohexane. In line with previous simulations^{29,30} and experiments,^{31,38} the proton transfers within few tens of femtoseconds from the oxygen to the nitrogen. Although the number of simulations is statistically small, the results suggest that the HBT simulation model is sufficiently accurate for the problem addressed here.

Cavity simulations

Up to ten HBT molecules (plus cyclohexane) were combined with up to 1,000 Rho molecules (plus water) and placed inside a cavity with an infinite Q-factor and a resonance that matches the absorption of both molecules. Table S1 provides an overview of the simulations. The largest system with 10 HBT and 1,000 Rho molecules contained 11,117,850 atoms (27,250 atoms at QM and 11,090,600 atoms at MM level), while the smallest system with 1 HBT and 100 Rho molecules contained 1,111,785 atoms (2,725 atom at QM and 1,109,060 atoms at MM level).

Figures S5 to S17 show how the contributions of the molecular excitations ($|\beta_i^K|^2$) and the cavity photon ($|\alpha^K|^2$) to the polaritonic states (K), in which the trajectories are running, evolve during *diabatic* surface hopping MD simulations of the various cavity-molecule systems. Also, the time evolution of the O-H distance in the HBT molecules is shown. In all simulations, the excitation of the optically accessible lower polariton is initially delocalized over *all* molecules *and* the confined light mode. However, within a few tens of femtoseconds the excitation localizes onto a *single* HBT molecule. Such localization is observed as a rapid rise to unity of the weight ($|\beta_i^0|^2$) of the state, in which HBT molecule i is photo-excited, to the total wave function (ψ_0 , equation 4), while the weights of the states, in which the other molecules ($|\beta_j^0|^2, j \neq i$) or the cavity are excited ($|\alpha^0|^2$), drop to zero. After localization of the excitation, the HBT molecule undergoes a rapid intra-molecular proton transfer to form the red-shifted photo-product. This electronically excited photo-product no longer couples with the confined light mode or with the other molecules, because the reduced S_0 - S_1 gap is no longer resonant with the cavity.

The localization of the excitation onto HBT molecule i is driven by thermal fluctuations that temporarily lower the energy of one of the dark states, in which the excitation is mostly localized on that HBT molecule ($|\beta_i^0|^2 \approx 1$), to a level below the energy of the lower polariton ($|\beta_i^0|^2 \approx 0.5/N$ and $|\alpha^0|^2 \approx 0.5$). Because of *non-adiabatic* coupling an avoided crossing opens up between these states along which the system can evolve *adiabatically* and remain in the lowest energy state. After *adiabatic* passage through an avoided crossing region, the excitation is localized on the HBT molecule ($|\beta_i^0|^2 \approx 1$) and triggers excited state proton transfer that brings the molecule out of resonance with the cavity. However, the coupling between these states is not always sufficiently strong to open up the avoided crossing. In these cases, a *real* crossing occurs instead and the

delocalized lower polaritonic state is maintained via a surface hop (dashed lines in Figures S5, S8, S9, S13, S14 and S16). Nevertheless, because there are very many regions of *non-adiabatic* coupling between the delocalized lower polariton and the localized state,³⁹ all cavity systems eventually end up in the lowest energy state localized on a single HBT molecule. Once the system has arrived into a state, in which the excitation is localized on a single HBT molecule, the ultra-fast excited-state intramolecular proton transfer reaction increases the gap with the lower polariton (Figure 1b in the main text) and prevents further transitions.

We repeated the simulations with the fewest switches surface hopping algorithm (Table S2). In figures S18 to S30 we plot: (i) the contributions of the molecular excitations ($|\beta_i^K|^2$) and the cavity photon ($|\alpha^K|^2$) to the polaritonic states (K) in which the trajectories are running; (ii) the O-H distances in the HBT molecule(s); (iii) the populations of the polaritonic states (*i.e.*, $c_K^*(t)c_K(t)$, equation 10); and (iv) the hopping probabilities. Because of the very high computational effort required to compute trajectories of such large systems, the total number of simulations is necessary lower than recommended for FSSH simulations.⁴⁰ Nevertheless, the results of the simulations yield a statically consistent picture that is in line with the results of the *diabatic* hopping simulations (Figures S5-S17): In all simulations, the excitation localizes within tens of femtoseconds onto a single HBT molecule, which then undergoes the photochemical reaction.

Table S1: Overview of *adiabatic* surface hopping simulations

simulation	HBT	Rho	Rabi split ^a	collapse	ESIPT ^b	Figure
1	10	1,000	0.53 eV	19 fs	65 fs	S5
2	5	500	0.47 eV	34 fs	58 fs	S6
3	5	500	0.47 eV	18 fs	107 fs	S7
4	1	100	0.43 eV	37 fs	196 fs	S8
5	1	100	0.44 eV	56 fs	108 fs	S9
6	1	100	0.43 eV	25 fs	53 fs	S10
7	1	100	0.41 eV	148 fs	192 fs	S11
8	1	100	0.41 eV	33 fs	177 fs	S12
9	1	100	0.43 eV	62 fs	174 fs	S13
10	1	100	0.43 eV	26 fs	138 fs	S14
11	1	100	0.44 eV	32 fs	80 fs	S15
12	1	100	0.41eV	19 fs	62 fs	S16
13	1	100	0.40 eV	95 fs	269 fs	S17

^a Rabi splitting at the start of the simulation

^b time at which the O-H distance exceeds 0.125 nm for the first time

Table S2: Overview of fewest switches surface hopping simulations

simulation	HBT	Rho	Rabi split ^a	collapse	ESIPT ^b	Figure
1	10	1,000	0.53 eV	53 fs	66 fs	S18
2	5	500	0.47 eV	38 fs	198 fs	S19
3	5	500	0.47 eV	18 fs	106 fs	S20
4	1	100	0.43 eV	49 fs	198 fs	S21
5	1	100	0.44 eV	17 fs	104 fs	S22
6	1	100	0.43 eV	17 fs	53 fs	S23
7	1	100	0.41 eV	148 fs	192 fs	S24
8	1	100	0.41 eV	33 fs	176 fs	S25
9	1	100	0.43 eV	62 fs	173 fs	S26
10	1	100	0.43 eV	11 fs	144 fs	S27
11	1	100	0.44 eV	50 fs	116 fs	S28
12	1	100	0.41 eV	19 fs	63 fs	S29
13	1	100	0.40 eV	44 fs	63 fs	S30

^a Rabi splitting at the start of the simulation

^b time at which the O-H distance exceeds 0.125 nm for the first time

Figures S1-S30

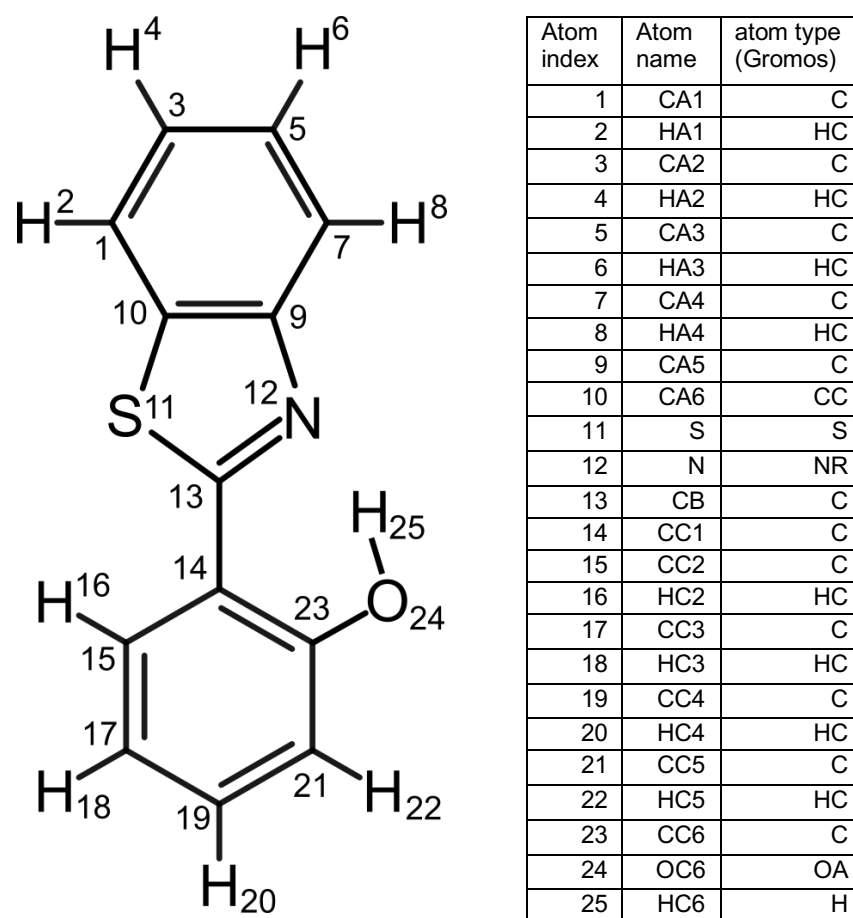


Figure S1: Atom names and types of the atoms in the hydroxyphenyl-benzothiazole (HBT) used in the MD simulations.

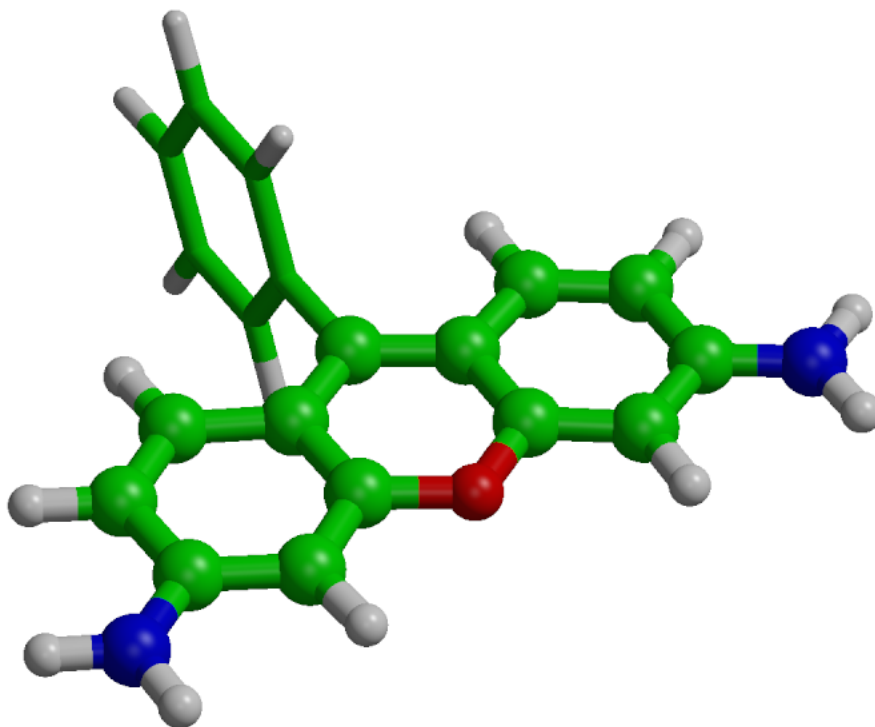


Figure S2: Rhodamine QM/MM model system.¹ The QM atoms, treated at the RHF/3-21G and CIS/3-21G levels of theory for the ground (S_0) and excited states (S_1), respectively, are shown in ball-and-stick representation, while the MM atoms, modeled with the Amber03 force field,¹⁷ are shown as sticks. The hydrogen link atom introduced along the bond on the QM/MM interface is not shown, and neither are the 3,684 TIP3P water molecules.¹⁹

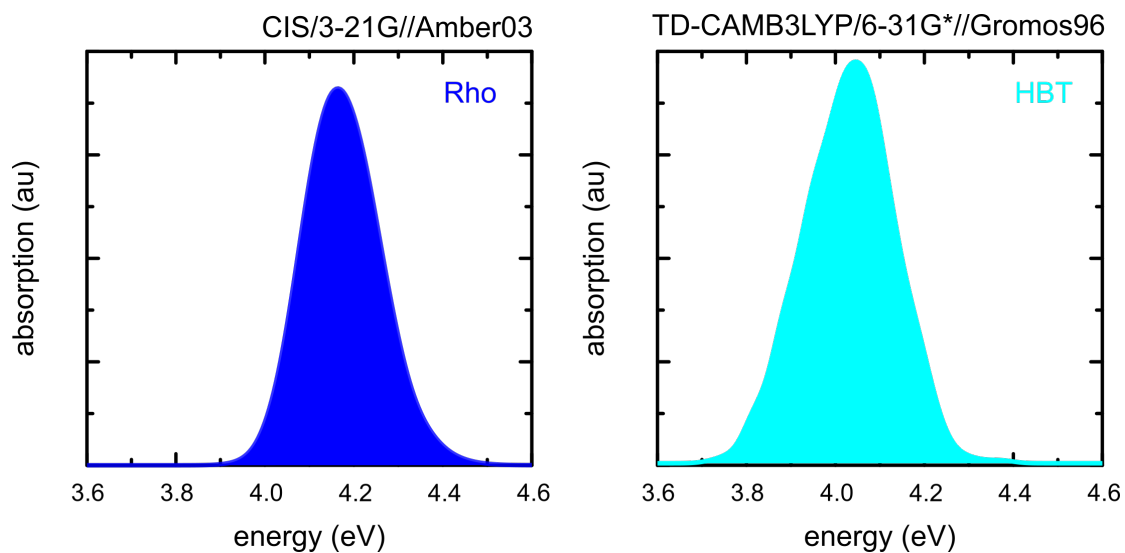


Figure S3: Absorption spectra of Rhodamine (left) and HBT (right) obtained by computing the vertical excitation energies in ensemble of ground state (S_0) configurations. For the Rhodamine model the S_0 to S_1 transitions were computed at the CIS level of theory with a 3-21G basis set²⁷ and the Amber03 force field¹⁷ for the water solvent. For HBT time-dependent density functional theory²⁸ was used with the CAMB3LYP functional²⁴⁻²⁶ and a 6-31G(d) basis set,²⁷ while the MM region, consisting of cyclohexane was modeled with the Gromos-2016H66 force field.¹⁸ The vertical excitation energies were convoluted with a Gaussian function with FWHM of 0.025 eV to generate the continuous spectra.

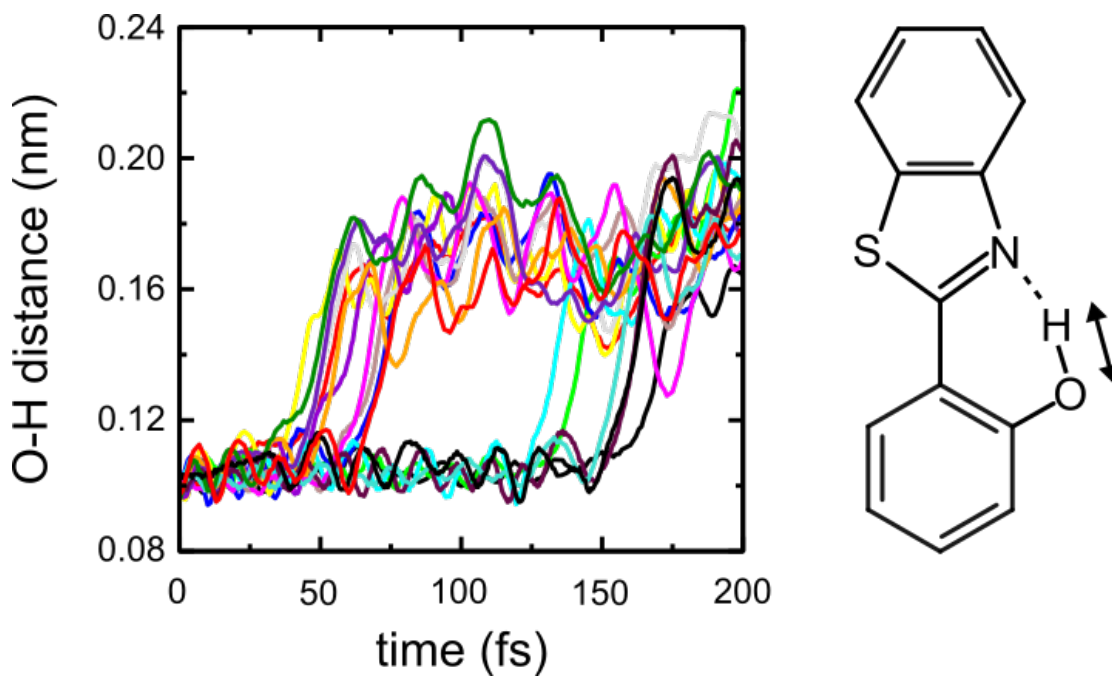


Figure S4: O-H distance as a function of time in 17 QM/MM MD trajectories of HBT after a resonant excitation into the S_1 state at 0 fs. Each color represents one trajectory. In these simulations, the S_1 energies and forces were calculated with time-dependent DFT,²⁸ using the CAMB3LYP functional²⁴⁻²⁶ in combination with the 6-31G(d) basis set.²⁷ The cyclohexane solvent was modeled with the Gromos-2016H66 force field.¹⁸

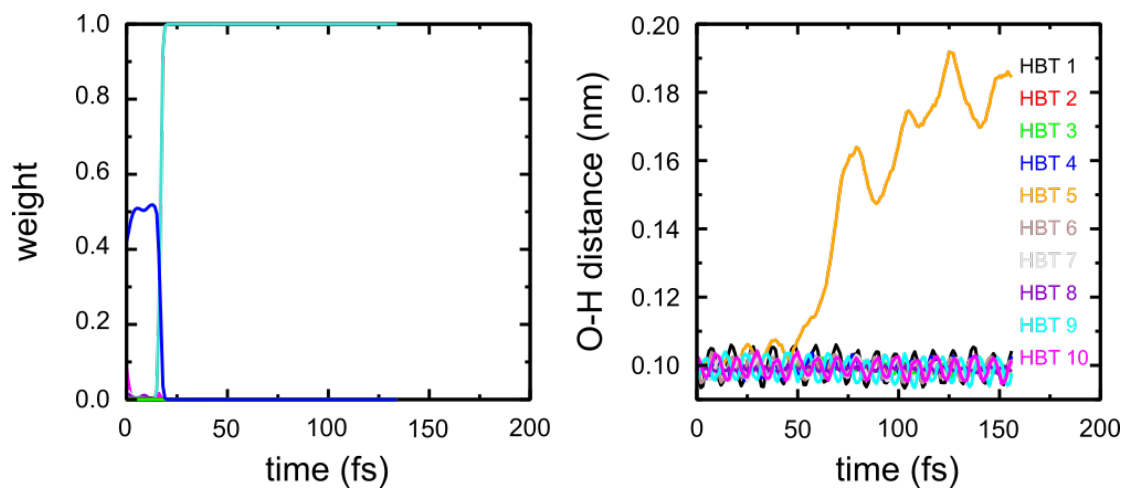


Figure S5: Time-evolution of the polaritonic state (left) and the O-H distance (right) in the HBT molecules during 200 fs of *diabatic* hopping MD simulation with 1,000 Rhodamines and 10 HBT molecules (plus environment) strongly coupled to confined light (simulation 1, Table S1). Left: weights of the excitations on each molecule ($|\beta_i^K|^2$, all colors) and of the confined light mode ($|\alpha^K|^2$, blue) to the polaritonic state (K) on which the 1,010-molecule trajectory evolves.

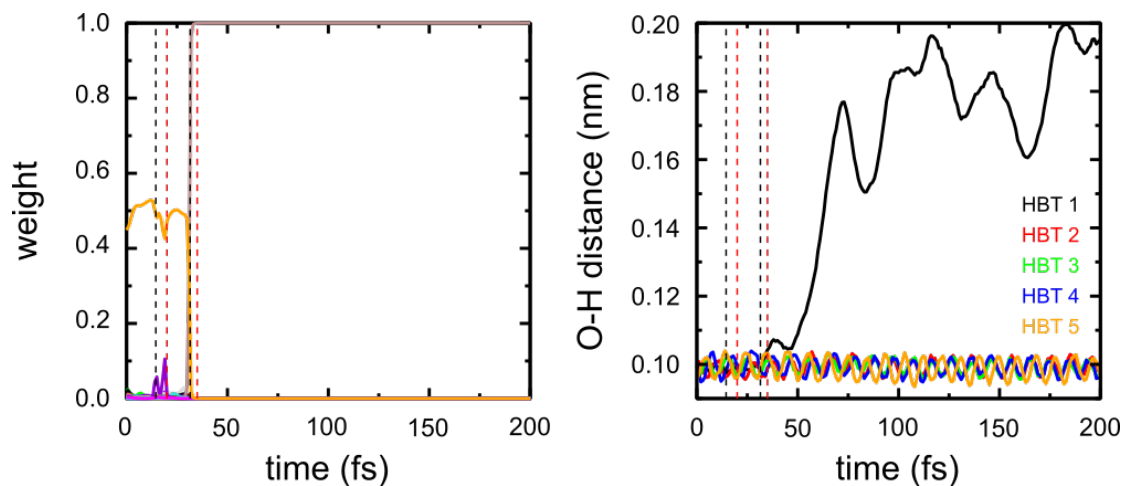


Figure S6: Time-evolution of the polaritonic state (left) and the O-H distance (right) in the HBT molecules during 200 fs of *diabatic* hopping MD simulation with 500 Rhodamines and 5 HBT molecules (plus environment) strongly coupled to confined light (simulation 2, Table S1). Left: weights of the excitations on each molecule ($|\beta_i^K|^2$, all colors) and of the confined light mode ($|\alpha^K|^2$, orange) to the polaritonic state (K) on which the 505-molecule trajectory evolves. *Diabatic* surface hops from the lowest energy state ($K = 0$) to the second-lowest state ($K = 1$) are indicated by black dashed lines, hops from 1 to 0 as red dashed lines.

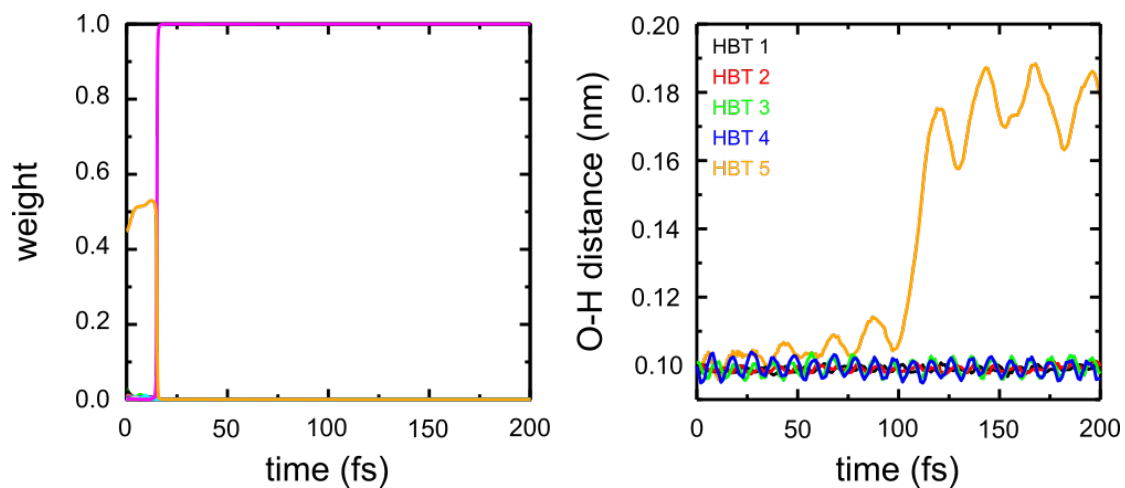


Figure S7: Time-evolution of the polaritonic state (left) and the O-H distance (right) in the HBT molecules during 200 fs of *diabatic* hopping MD simulation with 500 Rhodamines and 5 HBT molecules (plus environment) strongly coupled to confined light (simulation 3, Table S1). Left: weights of the excitations on each molecule ($|\beta_i^K|^2$, all colors) and of the confined light mode ($|\alpha^K|^2$, orange) to the polaritonic state (K) on which the 505-molecule trajectory evolves.

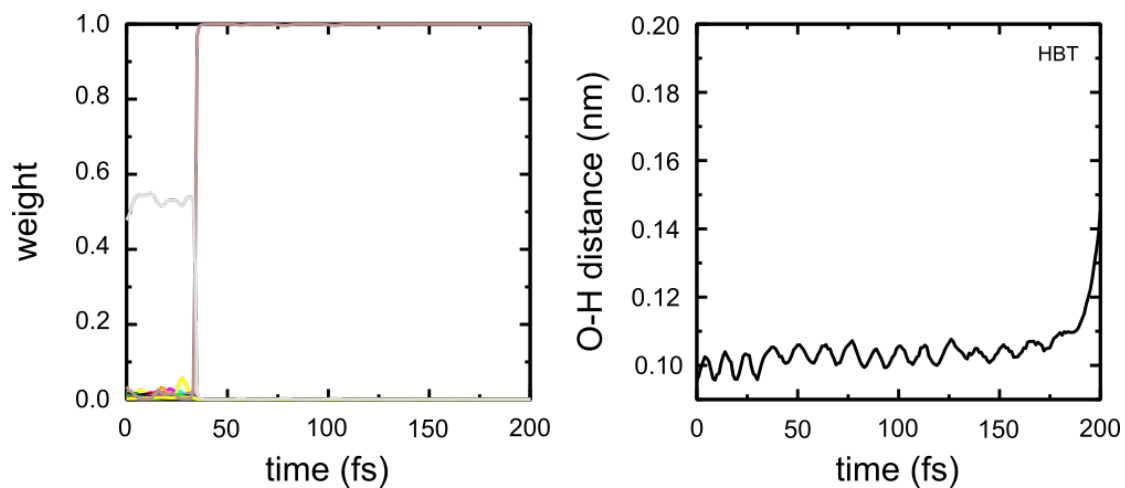


Figure S8: Time-evolution of the polaritonic state (left) and the O-H distance (right) in HBT during 200 fs of *diabatic* hopping MD simulation with 100 Rhodamines and 1 HBT molecule (plus environment) strongly coupled to confined light (simulation 4, Table S1). Left: weights of the excitations on each molecule ($|\beta_i^K|^2$, all colors) and of the confined light mode ($|\alpha^K|^2$, grey) to the polaritonic state (K) on which the 101-molecule trajectory evolves.

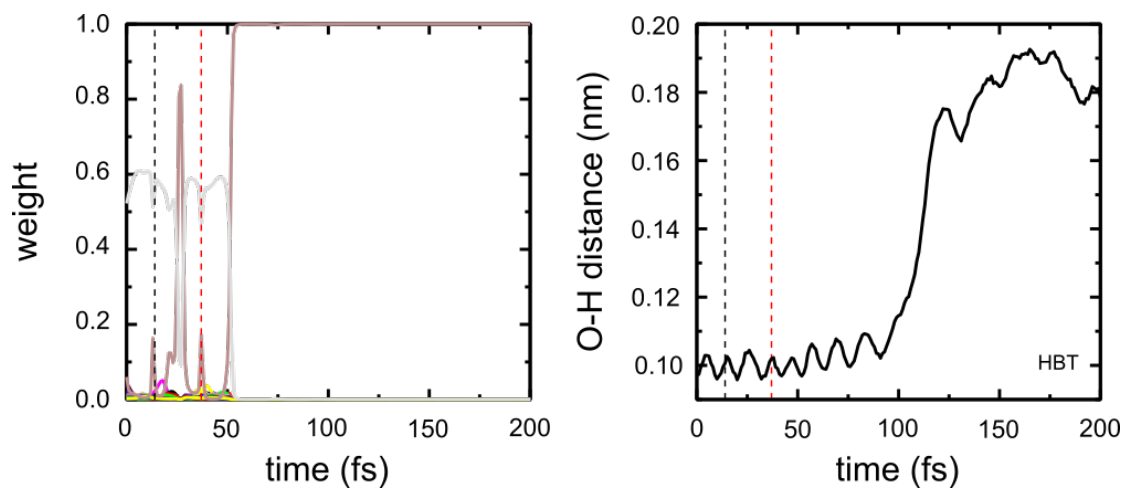


Figure S9: Time-evolution of the polaritonic state (left) and the O-H distance (right) in HBT during 200 fs of *diabatic* hopping MD simulation with 100 Rhodamines and 1 HBT molecule (plus environment) strongly coupled to confined light (simulation 5, Table S1). Left: weights of the excitations on each molecule ($|\beta_i^K|^2$, all colors) and of the confined light mode ($|\alpha^K|^2$, grey) to the polaritonic state (K) on which the 101-molecule trajectory evolves. *Diabatic* surface hops from the lowest energy state ($K = 0$) to the second-lowest state ($K = 1$) are indicated by black dashed lines, hops from 1 to 0 as red dashed lines.

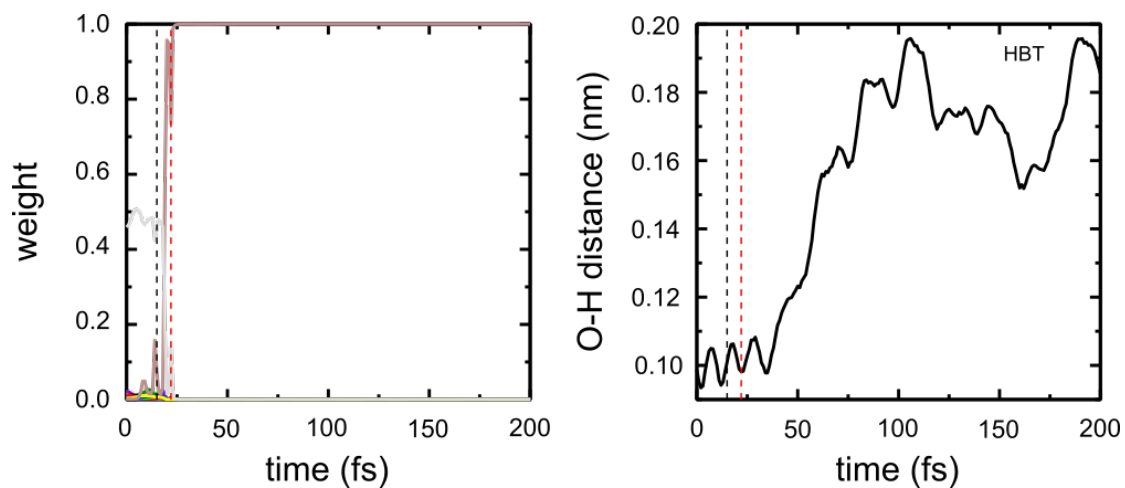


Figure S10: Time-evolution of the polaritonic state (left) and the O-H distance (right) in HBT during 200 fs of *adiabatic* hopping MD simulation with 100 Rhodamines and 1 HBT molecule (plus environment) strongly coupled to confined light (simulation 6, Table S1). Left: weights of the excitations on each molecule ($|\beta_i^K|^2$, all colors) and of the confined light mode ($|\alpha^K|^2$, grey) to the polaritonic state (K) on which the 101-molecule trajectory evolves.

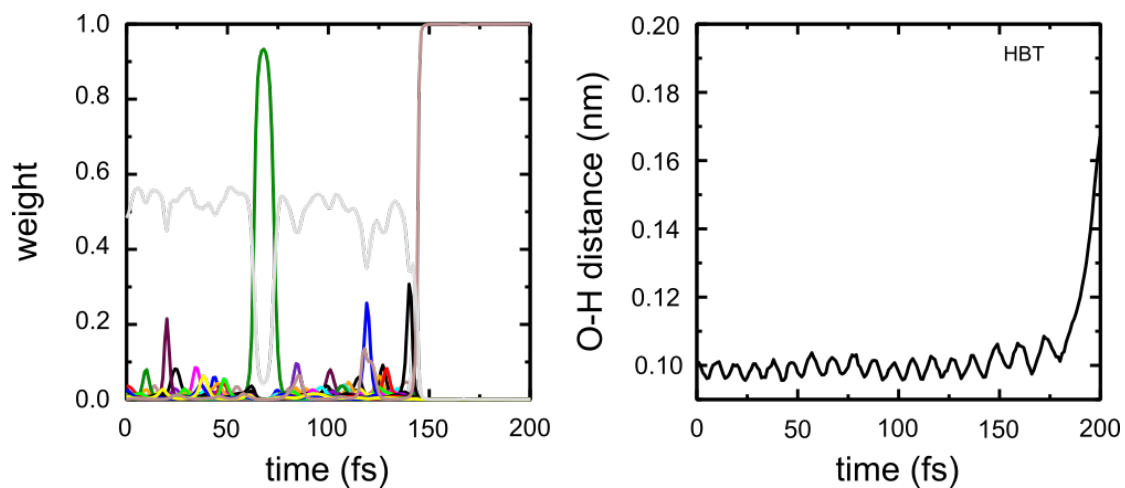


Figure S11: Time-evolution of the polaritonic state (left) and the O-H distance (right) in HBT during 200 fs of *diabatic* hopping MD simulation with 100 Rhodamines and 1 HBT molecule (plus environment) strongly coupled to confined light (simulation 7, Table S1). Left: weights of the excitations on each molecule ($|\beta_i^K|^2$, all colors) and of the confined light mode ($|\alpha^K|^2$, grey) to the polaritonic state (K) on which the 101-molecule trajectory evolves.

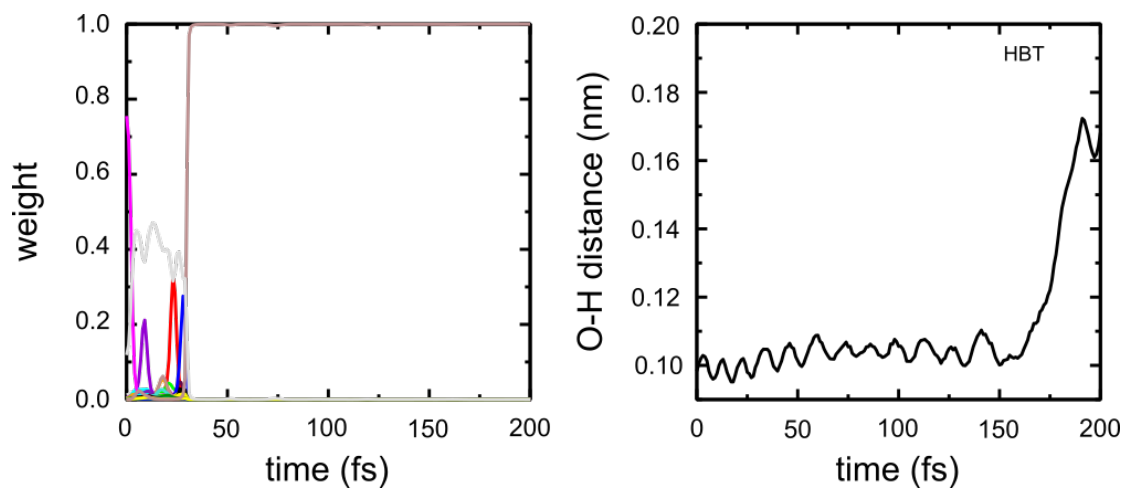


Figure S12: Time-evolution of the polaritonic state (left) and the O-H distance (right) in HBT during 200 fs of *adiabatic* hopping MD simulation with 100 Rhodamines and 1 HBT molecule (plus environment) strongly coupled to confined light (simulation 8, Table S1). Left: weights of the excitations on each molecule ($|\beta_i^K|^2$, all colors) and of the confined light mode ($|\alpha^K|^2$, grey) to the polaritonic state (K) on which the 101-molecule trajectory evolves.

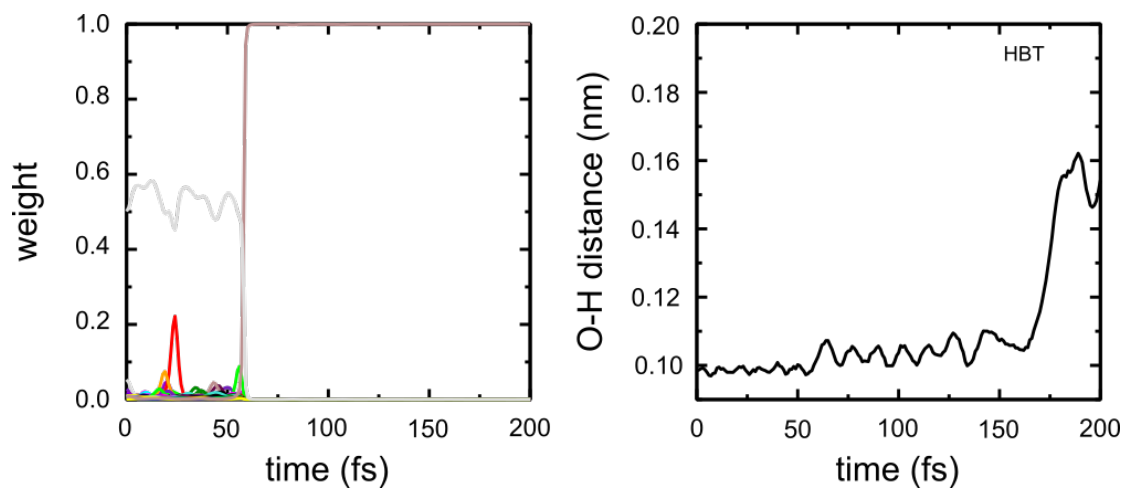


Figure S13: Time-evolution of the polaritonic state (left) and the O-H distance (right) in HBT during 200 fs of *adiabatic* hopping MD simulation with 100 Rhodamines and 1 HBT molecule (plus environment) strongly coupled to confined light (simulation 9, Table S1). Left: weights of the excitations on each molecule ($|\beta_i^K|^2$, all colors) and of the confined light mode ($|\alpha^K|^2$, grey) to the polaritonic state (K) on which the 101-molecule trajectory evolves.

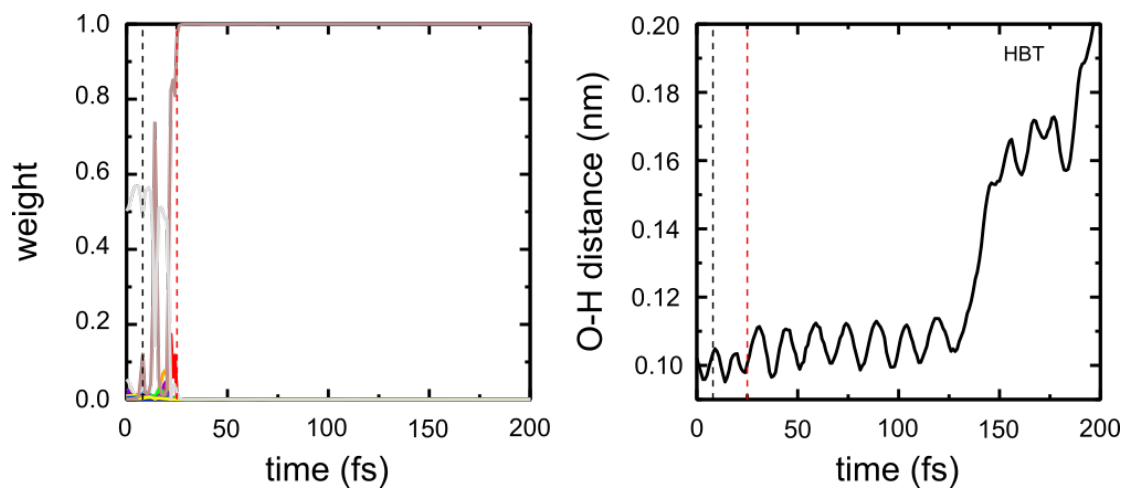


Figure S14: Time-evolution of the polaritonic state (left) and the O-H distance (right) in HBT during 200 fs of *diabatic* hopping MD simulation with 100 Rhodamines and 1 HBT molecule (plus environment) strongly coupled to confined light (simulation 10, Table S1). Left: weights of the excitations on each molecule ($|\beta_i^K|^2$, all colors) and of the confined light mode ($|\alpha^K|^2$, grey) to the polaritonic state (K) on which the 101-molecule trajectory evolves. *Diabatic* surface hops from the lowest energy state ($K = 0$) to the second-lowest state ($K = 1$) are indicated by black dashed lines, hops from 1 to 0 as red dashed lines.

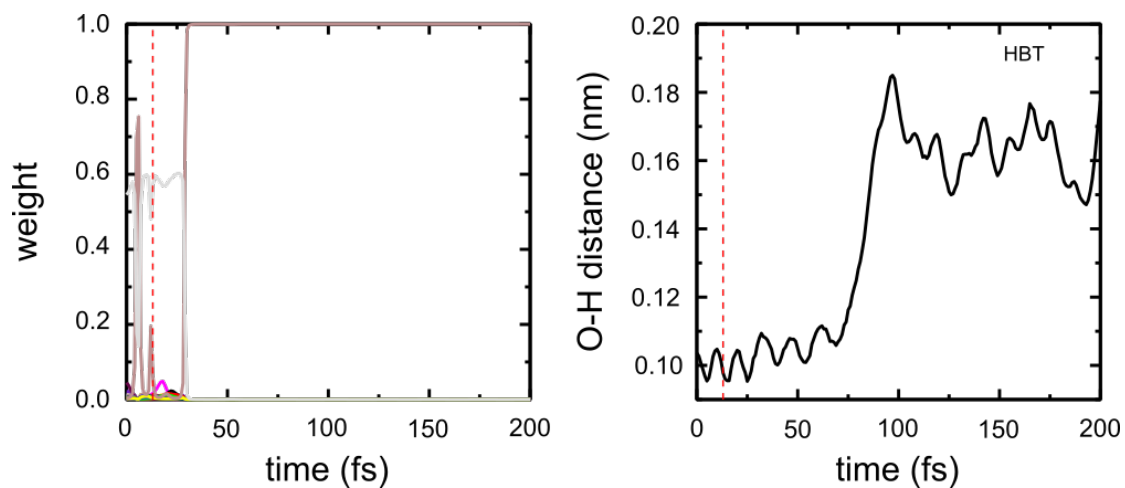


Figure S15: Time-evolution of the polaritonic state (left) and the O-H distance (right) in HBT during 200 fs of *diabatic* hopping MD simulation with 100 Rhodamines and 1 HBT molecule (plus environment) strongly coupled to confined light (simulation 11, Table S1). Left: weights of the excitations on each molecule ($|\beta_i^K|^2$, all colors) and of the confined light mode ($|\alpha^K|^2$, grey) to the polaritonic state (K) on which the 101-molecule trajectory evolves. *Diabatic* surface hops from the second-lowest energy state ($K = 1$, the lower polariton at 0 fs) to the lowest state ($K = 0$) are indicated by red dashed lines.

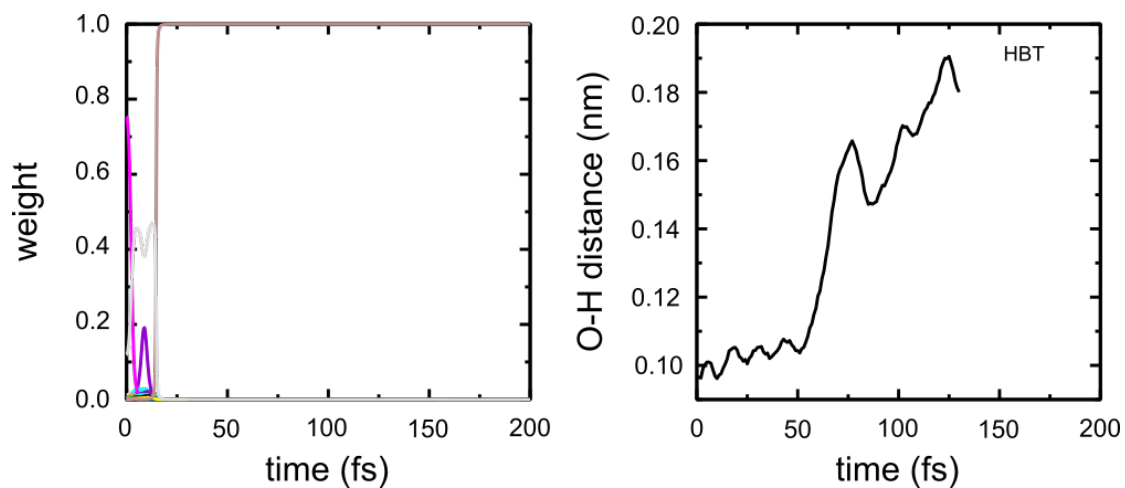


Figure S16: Time-evolution of the polaritonic state (left) and the O-H distance (right) in HBT during 200 fs of *diabatic* hopping MD simulation with 100 Rhodamines and 1 HBT molecule (plus environment) strongly coupled to confined light (simulation 12, Table S1). Left: weights of the excitations on each molecule ($|\beta_i^K|^2$, all colors) and of the confined light mode ($|\alpha^K|^2$, grey) to the polaritonic state (K) on which the 101-molecule trajectory evolves. *Diabatic* surface hops from the lowest energy state ($K = 0$) to the second-lowest state ($K = 1$) are indicated by black dashed lines, hops from 1 to 0 as red dashed lines.

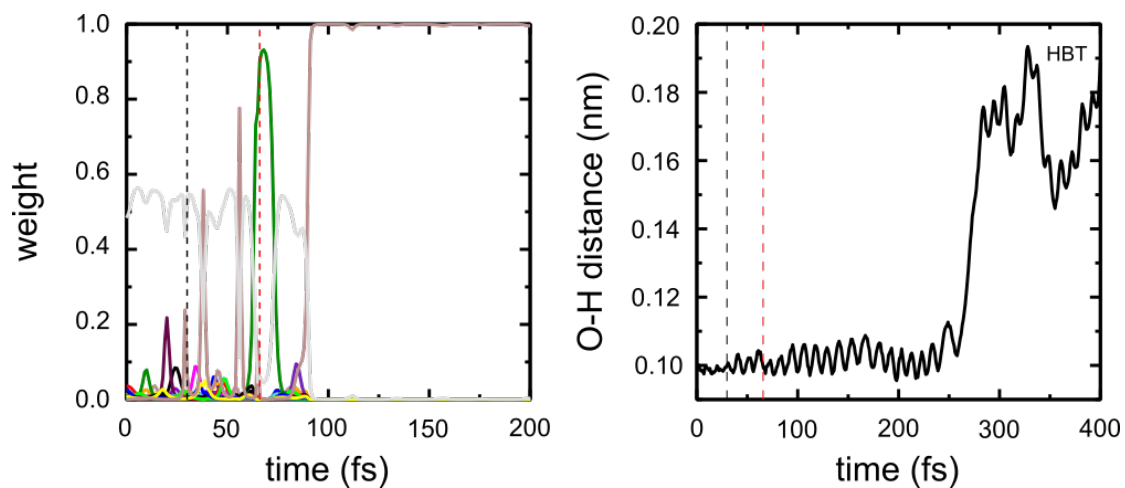


Figure S17: Time-evolution of the polaritonic state (left) and the O-H distance (right) in HBT during 200 fs of *diabatic* hopping MD simulation with 100 Rhodamines and 1 HBT molecule (plus environment) strongly coupled to confined light (simulation 13, Table S1). Left: weights of the excitations on each molecule ($|\beta_i^K|^2$, all colors) and of the confined light mode ($|\alpha^K|^2$, grey) to the polaritonic state (K) on which the 101-molecule trajectory evolves.

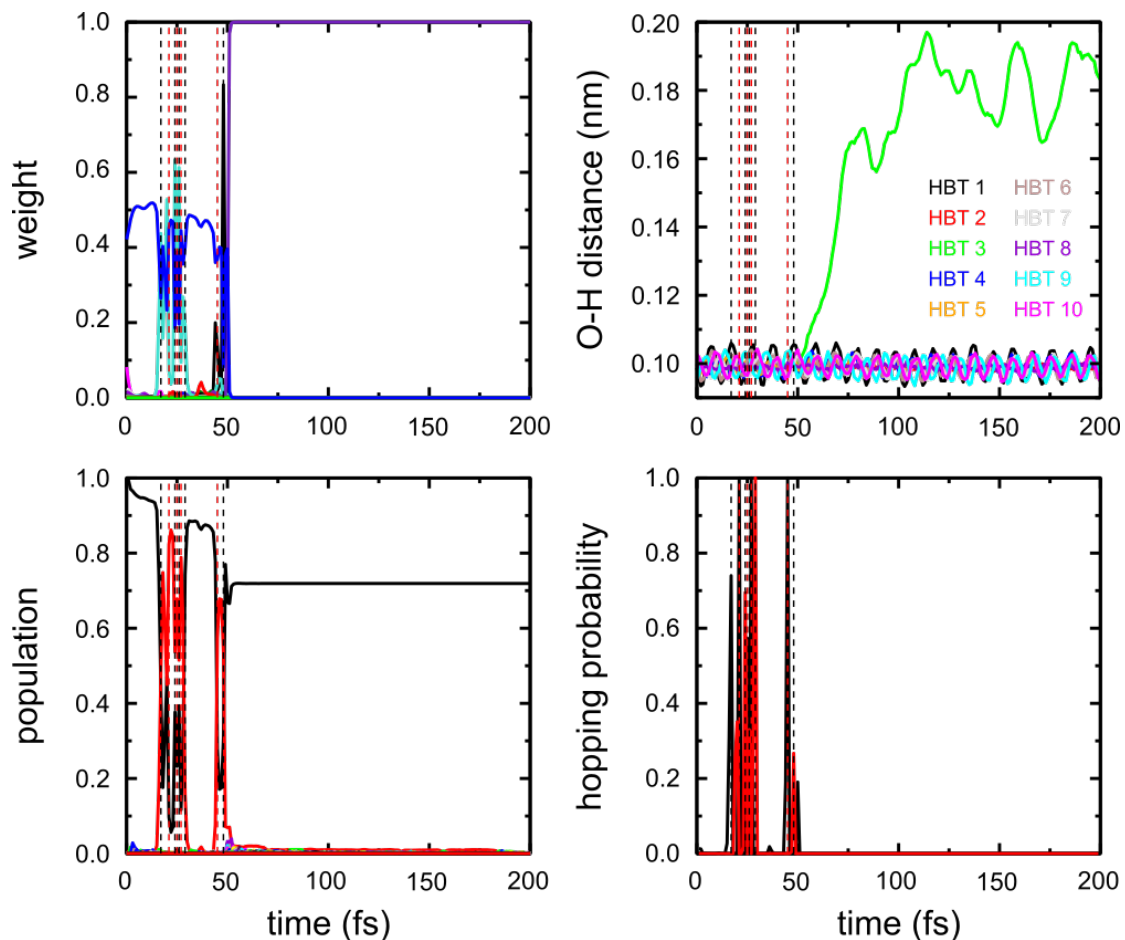


Figure S18: time-evolution of the polaritonic state and the O-H distance (top right) in the HBT molecules during 200 fs of FSSH MD simulation with 1,000 Rhodamines and 10 HBT molecules (plus environment) strongly coupled to confined light (simulation 1, Table S2). Top left: weights of the excitations on each molecule ($|\beta_i^K|^2$, all colors) and of the confined light mode ($|\alpha^K|^2$, blue) to the polaritonic state (K) on which the 1,010-molecule trajectory evolves. Bottom left: populations of the 1,011 polaritonic states ($c(t)_K^* c(t)_K$, equation 9). State of lowest energy ($K = 0$) in black, second-lowest ($K = 1$) in red, third-lowest ($K = 2$) in green, etc. Bottom right: hopping probabilities (equation 13) for transition from state 0 into state 1 (black) and back (red). Surface hops from state 0 to 1 are indicated by black dashed lines, hops from 1 to 0 as red dashed lines.

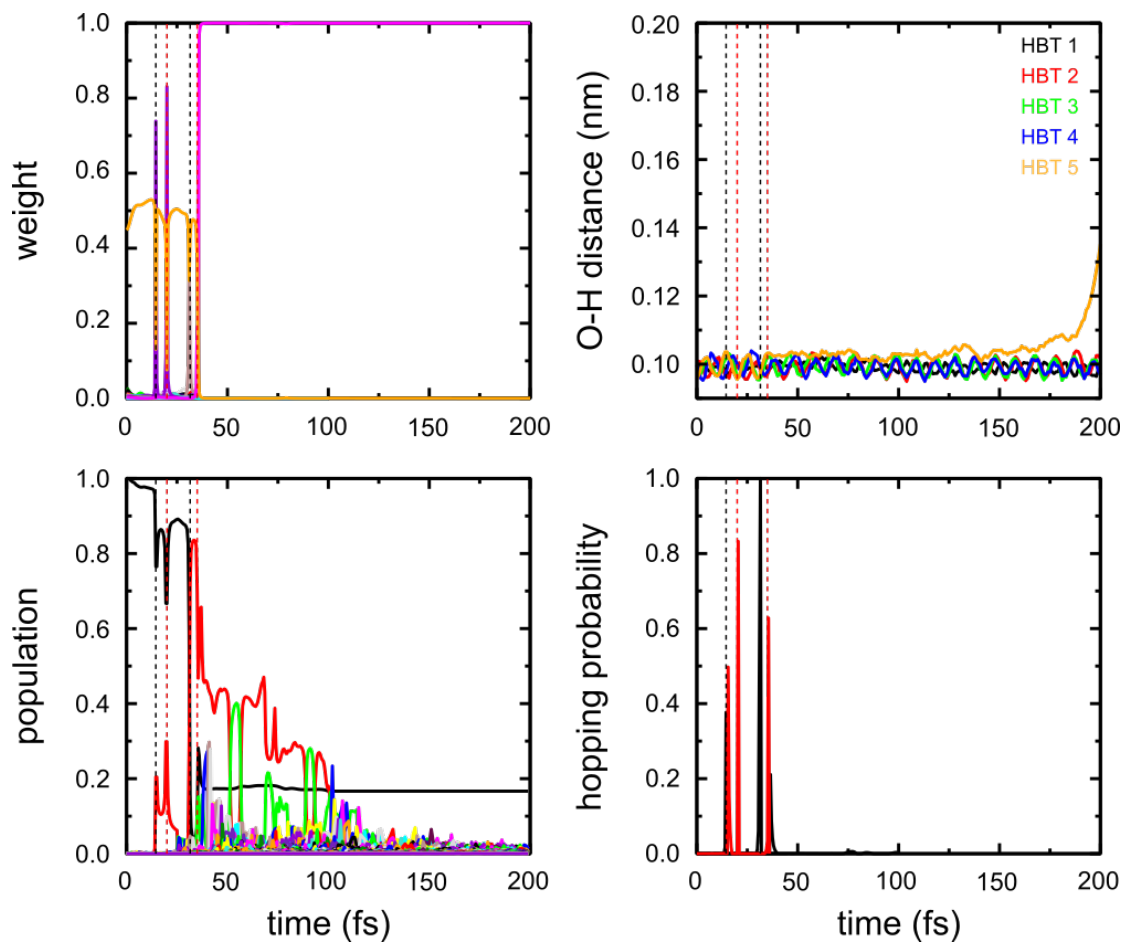


Figure S19: Time-evolution of the polaritonic state and the O-H distance (top right) in the HBT molecules during 200 fs of FSSH MD simulation with 500 Rhodamines and 5 HBT molecules (plus environment) strongly coupled to confined light (simulation 2, Table S2). Top left: weights of the excitations on each molecule ($|\beta_i^K|^2$, all colors) and of the confined light mode ($|\alpha^K|^2$, orange) of the polaritonic state (K) on which the 505-molecule trajectory evolves. Bottom left: populations of the 506 polaritonic states ($c(t)_K^* c(t)_K$, equation 9). State of lowest energy ($K = 0$) in black, second-lowest ($K = 1$) in red, third-lowest ($K = 2$) in green, etc. Bottom right: hopping probabilities (equation 13) for transition from state 0 into state 1 (black) and back (red). Surface hops from state 0 to 1 are indicated by black dashed lines, hops from 1 to 0 as red dashed lines.

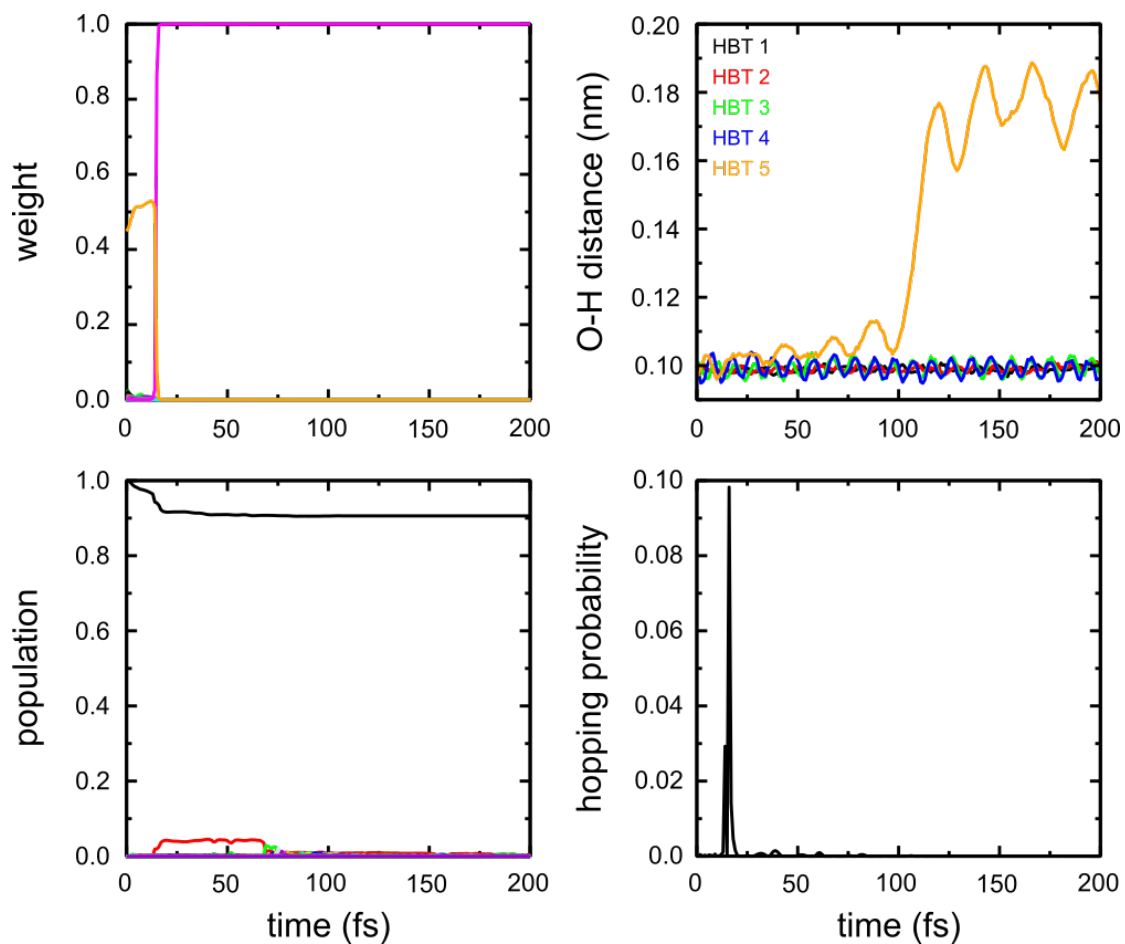


Figure S20: time-evolution of the polaritonic state and the O-H distance (top right) in the HBT molecules during 200 fs of FSSH MD simulation with 500 Rhodamines and 5 HBT molecules (plus environment) strongly coupled to confined light (simulation 3, Table S2). Top left: weights of the excitations on each molecule ($|\beta_i^K|^2$, all colors) and of the confined light mode ($|\alpha^K|^2$, orange) of the polaritonic state (K) on which the 505-molecule trajectory evolves. Bottom left: populations of the 506 polaritonic states ($c(t)_K^* c(t)_K$, equation 9). State of lowest energy ($K = 0$) in black, second-lowest ($K = 1$) in red, third-lowest ($K = 2$) in green, etc. Bottom right: hopping probabilities (equation 13) for transition from state 0 into state 1 (black).

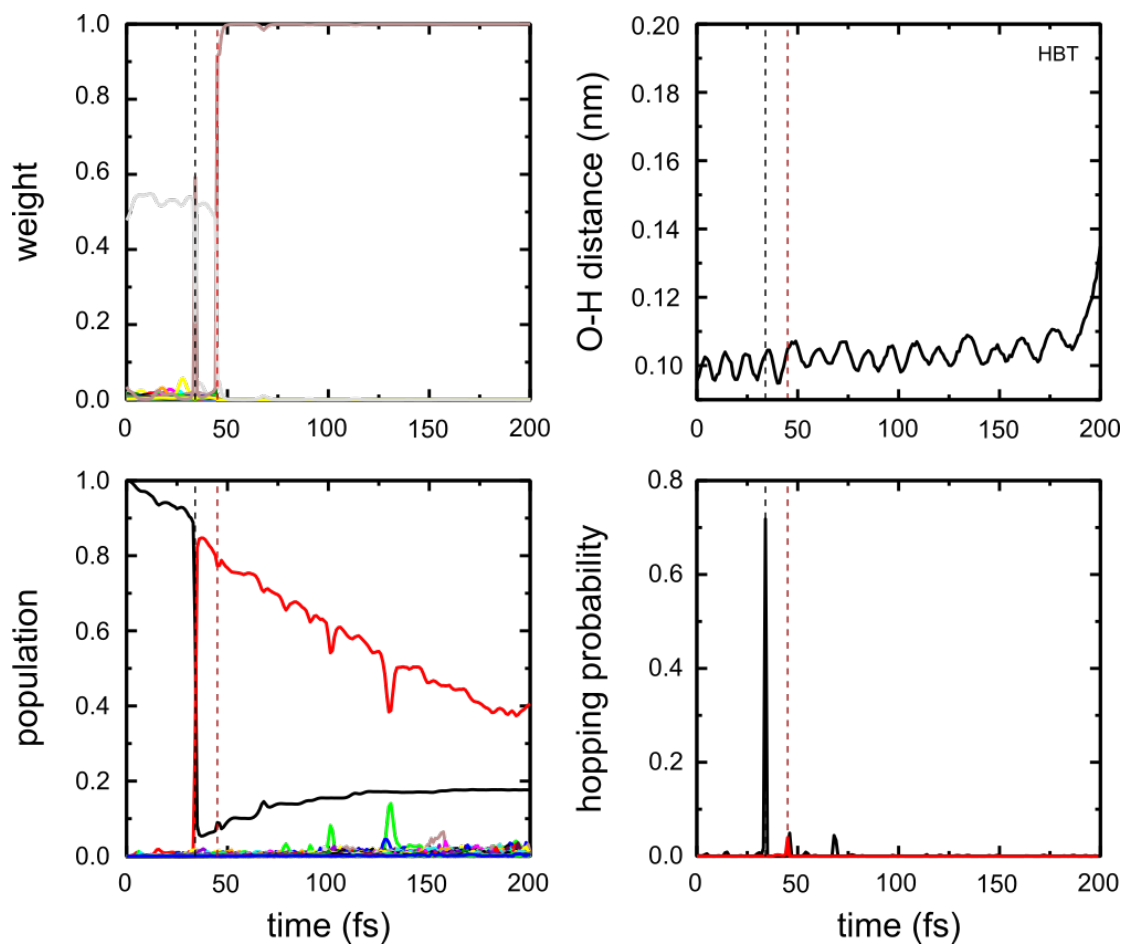


Figure S21: Time-evolution of the polaritonic state and the O-H distance (top right) in HBT during 200 fs of FSSH MD simulation with 100 Rhodamines and 1 HBT molecule (plus environment) strongly coupled to confined light (simulation 4, Table S2). Top left: weights of the excitations on each molecule ($|\beta_i^K|^2$, all colors) and of the confined light mode ($|\alpha^K|^2$, grey) of the polaritonic state (K) on which the 101-molecule trajectory evolves. Bottom left: populations of the 102 polaritonic states ($c(t)_K^* c(t)_K$, equation 9). State of lowest energy ($K = 0$) in black, second-lowest ($K = 1$) in red, third-lowest ($K = 2$) in green, etc. Bottom right: hopping probabilities (equation 13) for transition from state 0 into state 1 (black) and back (red). Surface hops from state 0 to 1 are indicated by black dashed lines, hops from 1 to 0 as red dashed lines.

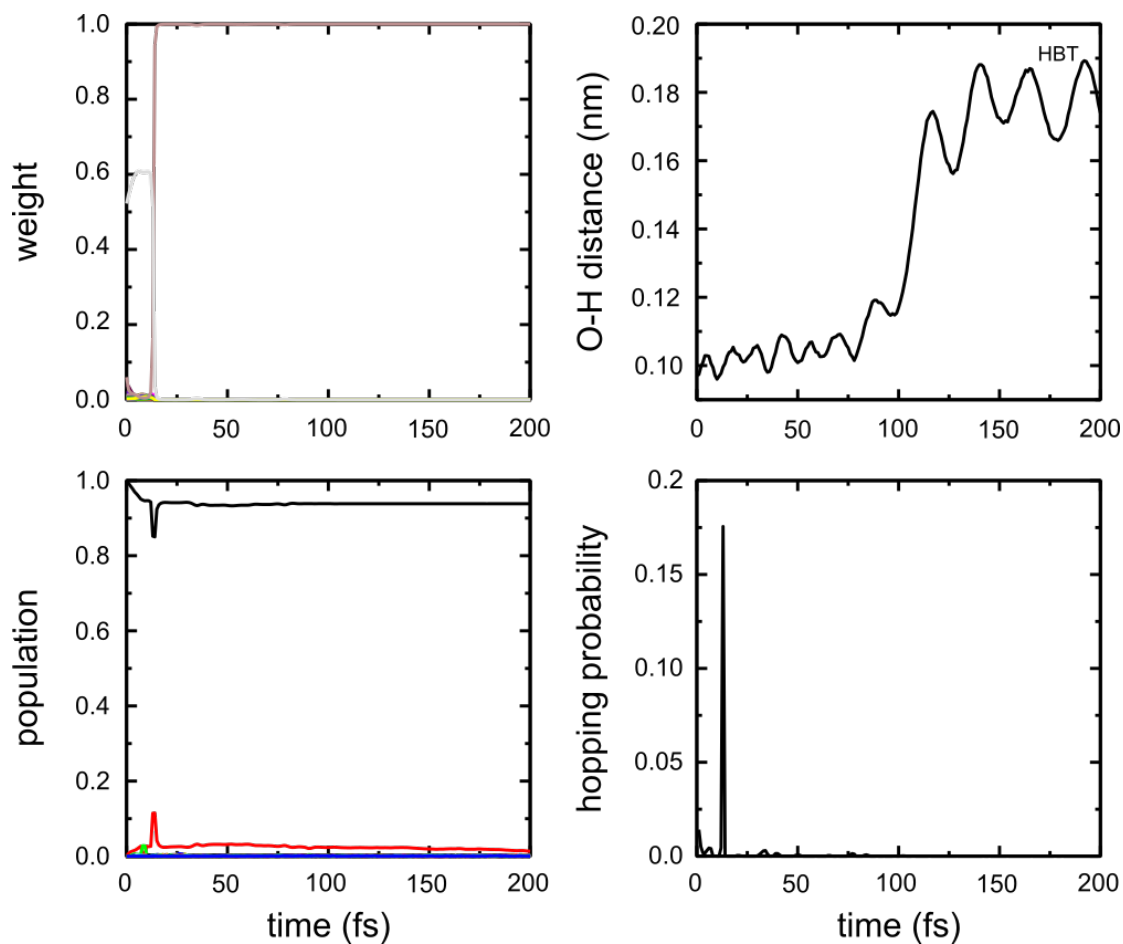


Figure S22: Time-evolution of the polaritonic state and the O-H distance (top right) in HBT during 200 fs of FSSH MD simulation with 100 Rhodamines and 1 HBT molecule (plus environment) strongly coupled to confined light (simulation 5, Table S2). Top left: weights of the excitations on each molecule ($|\beta_i^K|^2$, all colors) and of the confined light mode ($|\alpha^K|^2$, grey) of the polaritonic state (K) on which the 101-molecule trajectory evolves. Bottom left: populations of the 102 polaritonic states ($c(t)_K^* c(t)_K$, equation 9). State of lowest energy ($K = 0$) in black, second-lowest ($K = 1$) in red, third-lowest ($K = 2$) in green, etc. Bottom right: hopping probabilities (equation 13) for transition from state 0 into state 1 (black).

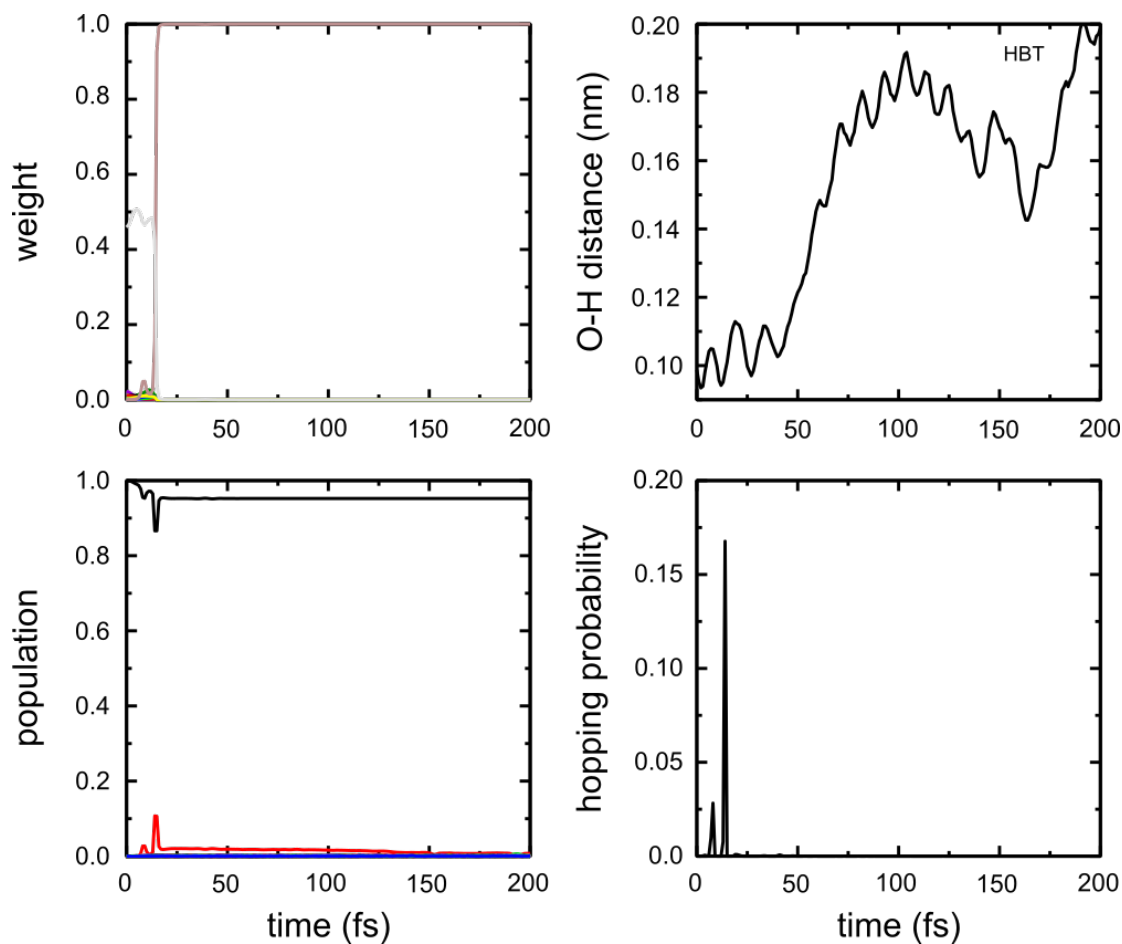


Figure S23: Time-evolution of the polaritonic state and the O-H distance (top right) in HBT during 200 fs of FSSH MD simulation with 100 Rhodamines and 1 HBT molecule (plus environment) strongly coupled to confined light (simulation 6, Table S2). Top left: weights of the excitations on each molecule ($|\beta_i^K|^2$, all colors) and of the confined light mode ($|\alpha^K|^2$, grey) of the polaritonic state (K) on which the 101-molecule trajectory evolves. Bottom left: populations of the 102 polaritonic states ($c(t)_K^* c(t)_K$, equation 9). State of lowest energy ($K = 0$) in black, second-lowest ($K = 1$) in red, third-lowest ($K = 2$) in green, etc. Bottom right: hopping probabilities (equation 13) for transition from state 0 into state 1 (black).

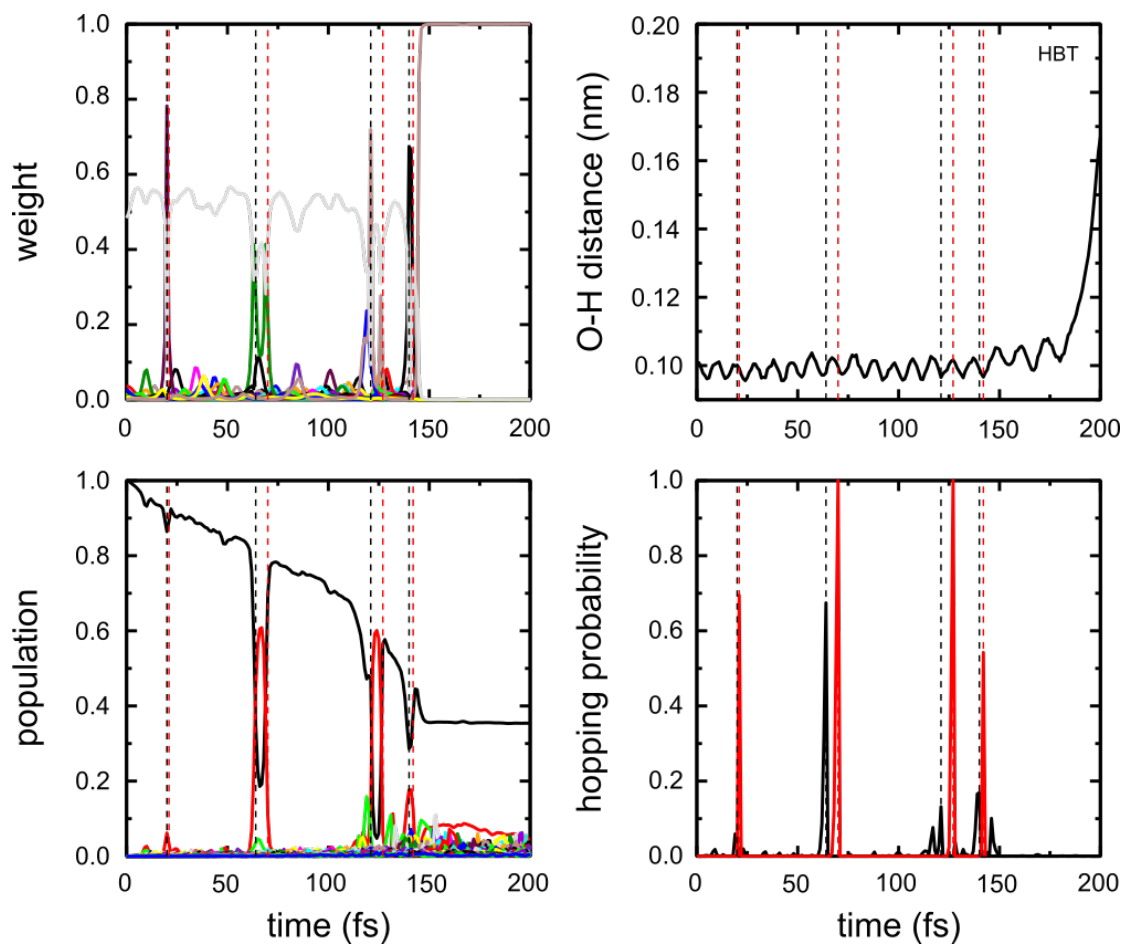


Figure S24: Time-evolution of the polaritonic state and the O-H distance (top right) in HBT during 200 fs of FSSH MD simulation with 100 Rhodamines and 1 HBT molecule (plus environment) strongly coupled to confined light (simulation 7, Table S2). Top left: weights of the excitations on each molecule ($|\beta_i^K|^2$, all colors) and of the confined light mode ($|\alpha^K|^2$, grey) of the polaritonic state (K) on which the 101-molecule trajectory evolves. Bottom left: populations of the 102 polaritonic states ($c(t)_K^* c(t)_K$, equation 9). State of lowest energy ($K = 0$) in black, second-lowest ($K = 1$) in red, third-lowest ($K = 2$) in green, etc. Bottom right: hopping probabilities (equation 13) for transition from state 0 into state 1 (black) and back (red). Surface hops from state 0 to 1 are indicated by black dashed lines, hops from 1 to 0 as red dashed lines.

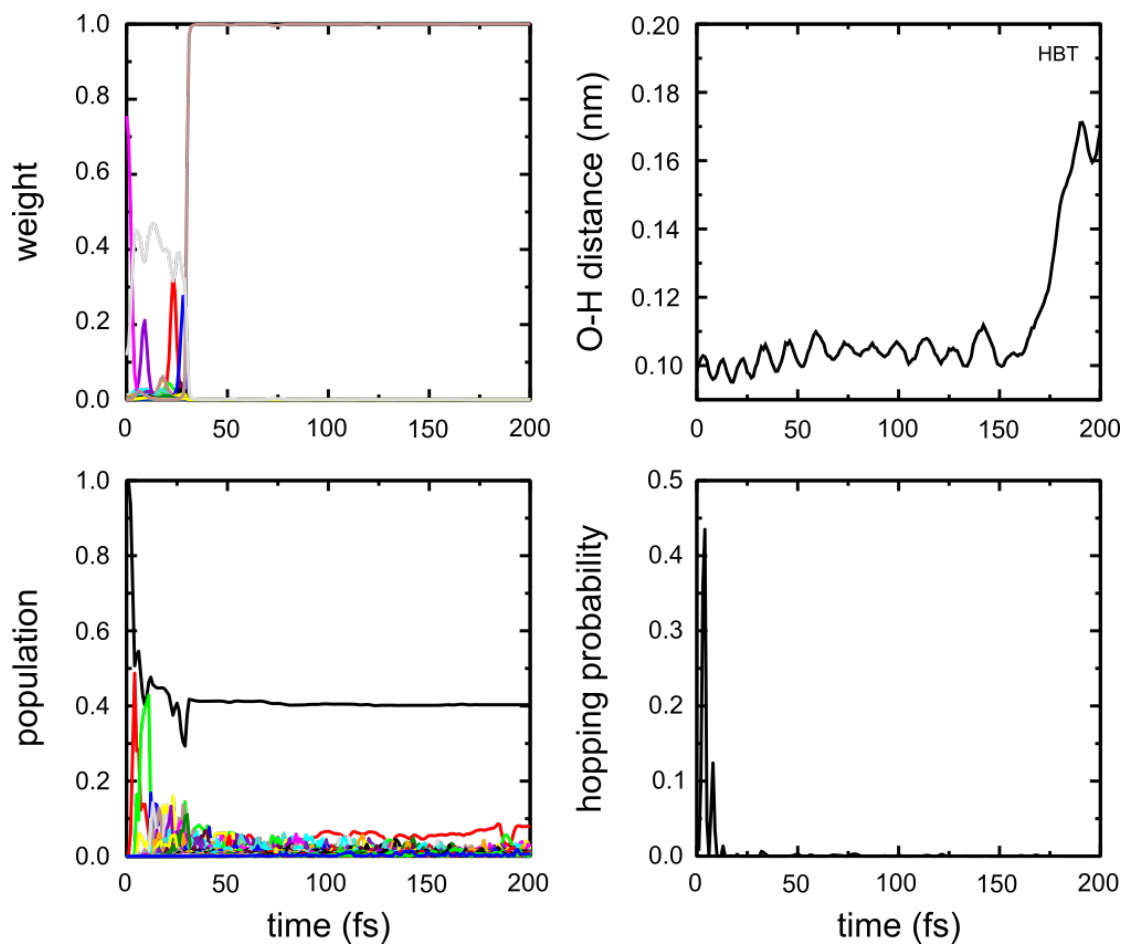


Figure S25: Time-evolution of the polaritonic state and the O-H distance (top right) in HBT during 200 fs of FSSH MD simulation with 100 Rhodamines and 1 HBT molecule (plus environment) strongly coupled to confined light (simulation 8, Table S2). Top left: weights of the excitations on each molecule ($|\beta_i^K|^2$, all colors) and of the confined light mode ($|\alpha^K|^2$, grey) of the polaritonic state (K) on which the 101-molecule trajectory evolves. Bottom left: populations of the 102 polaritonic states ($c(t)_K^* c(t)_K$, equation 9). State of lowest energy ($K = 0$) in black, second-lowest ($K = 1$) in red, third-lowest ($K = 2$) in green, etc. Bottom right: hopping probabilities (equation 13) for transition from state 0 into state 1 (black).

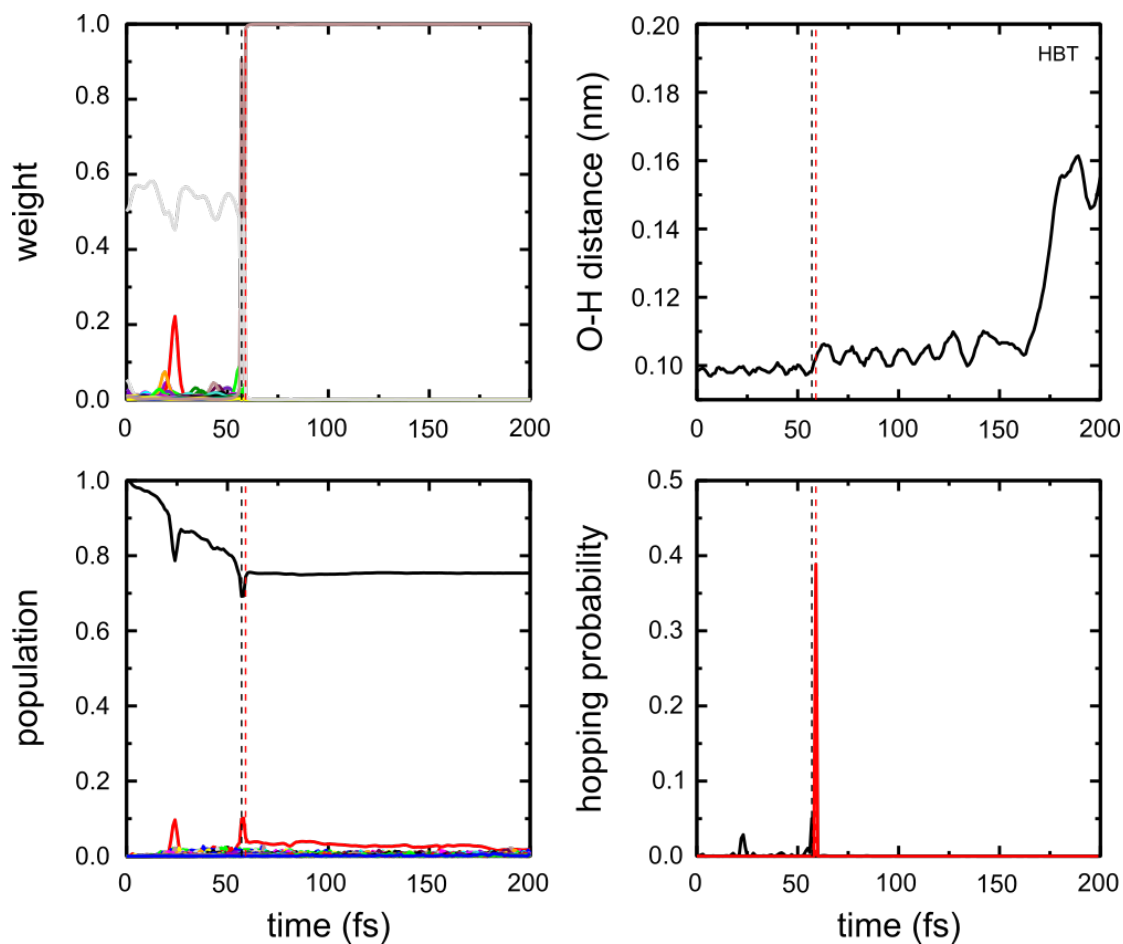


Figure S26: Time-evolution of the polaritonic state and the O-H distance (top right) in HBT during 200 fs of FSSH MD simulation with 100 Rhodamines and 1 HBT molecule (plus environment) strongly coupled to confined light (simulation 9, Table S2). Top left: weights of the excitations on each molecule ($|\beta_i^K|^2$, all colors) and of the confined light mode ($|\alpha^K|^2$, grey) of the polaritonic state (K) on which the 101-molecule trajectory evolves. Bottom left: populations of the 102 polaritonic states ($c(t)_K^* c(t)_K$, equation 9). State of lowest energy ($K = 0$) in black, second-lowest ($K = 1$) in red, third-lowest ($K = 2$) in green, etc. Bottom right: hopping probabilities (equation 13) for transition from state 0 into state 1 (black) and back (red). Surface hops from state 0 to 1 are indicated by black dashed lines, hops from 1 to 0 as red dashed lines.

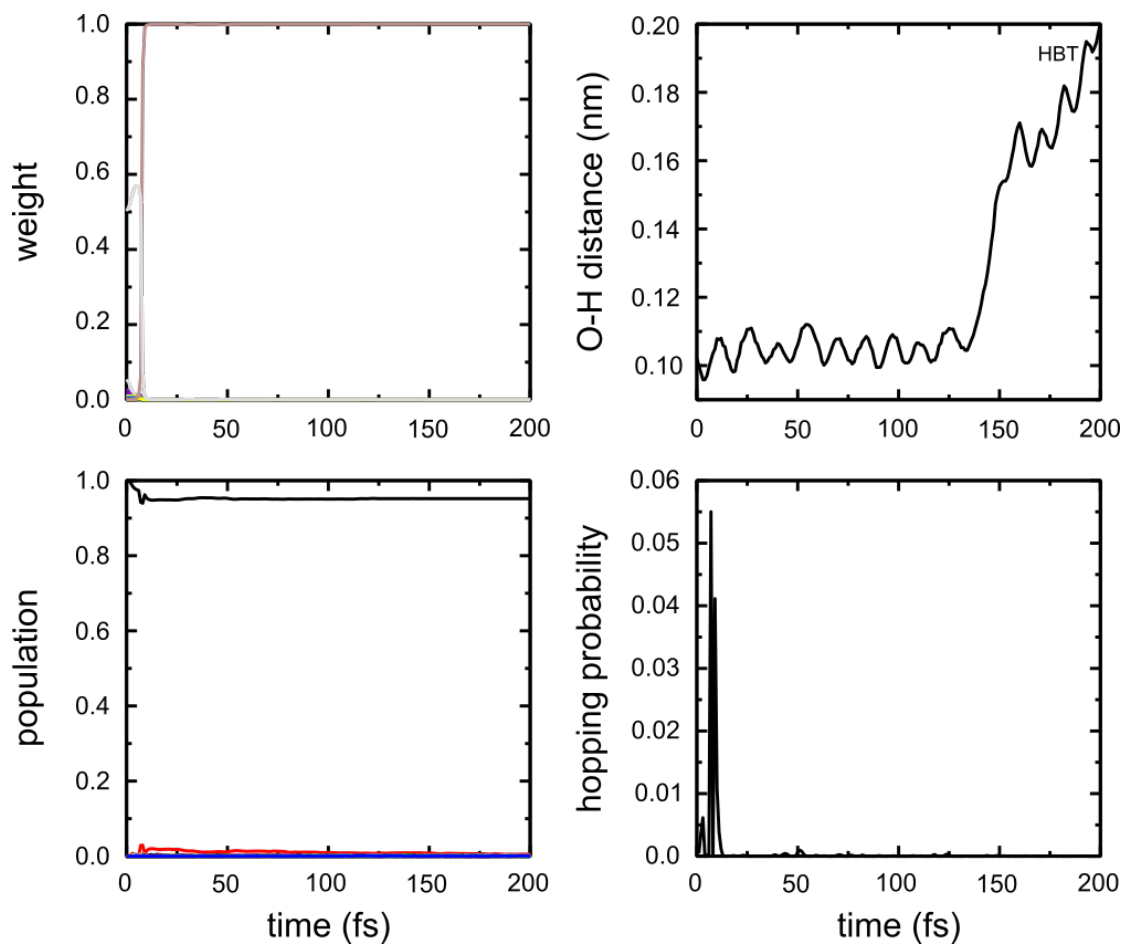


Figure S27: Time-evolution of the polaritonic state and the O-H distance (top right) in HBT during 200 fs of FSSH MD simulation with 100 Rhodamines and 1 HBT molecule (plus environment) strongly coupled to confined light (simulation 10, Table S2). Top left: weights of the excitations on each molecule ($|\beta_i^K|^2$, all colors) and of the confined light mode ($|\alpha^K|^2$, grey) of the polaritonic state (K) on which the 101-molecule trajectory evolves. Bottom left: populations of the 102 polaritonic states ($c(t)_K^* c(t)_K$, equation 9). State of lowest energy ($K = 0$) in black, second-lowest ($K = 1$) in red, third-lowest ($K = 2$) in green, etc. Bottom right: hopping probabilities (equation 13) for transition from state 0 into state 1 (black).

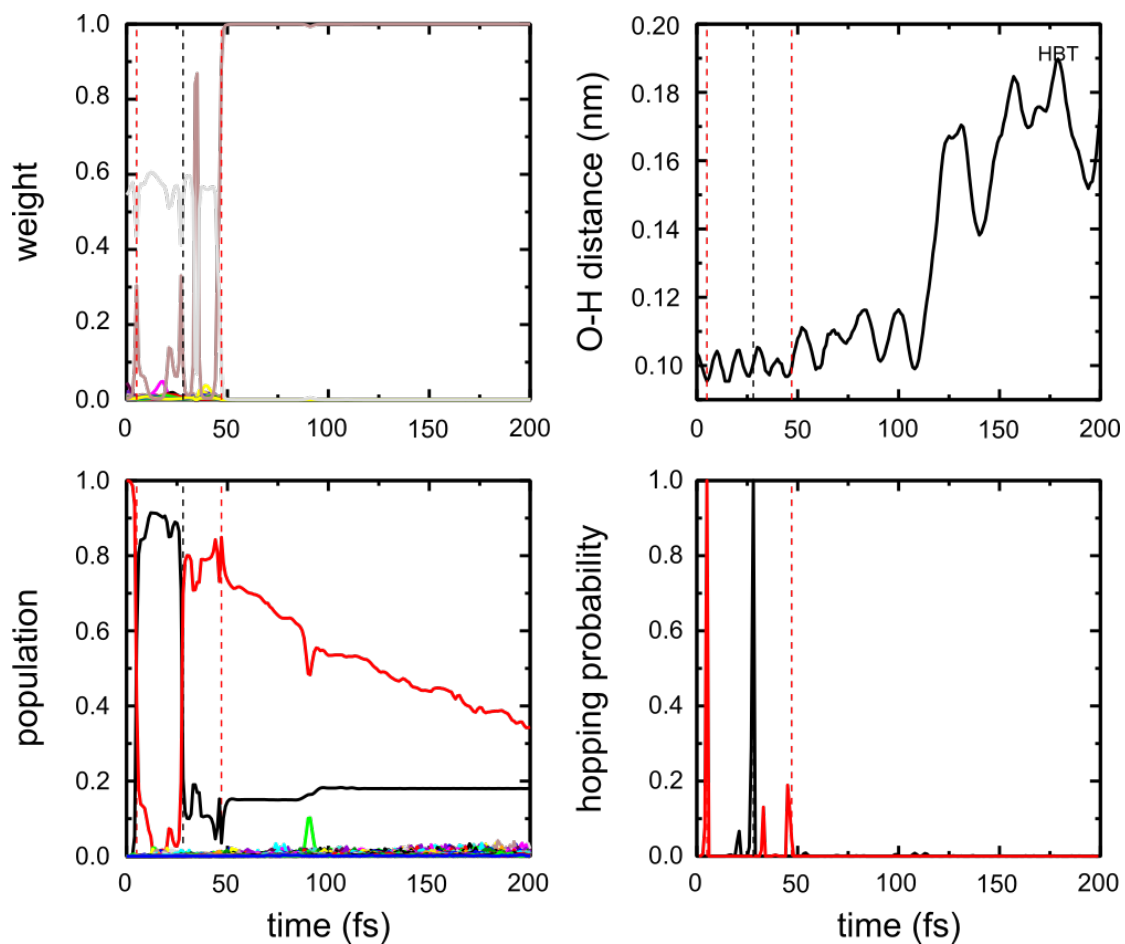


Figure S28: Time-evolution of the polaritonic state and the O-H distance (top right) in HBT during 200 fs of FSSH MD simulation with 100 Rhodamines and 1 HBT molecule (plus environment) strongly coupled to confined light (simulation 11 Table S2). Top left: weights of the excitations on each molecule ($|\beta_i^K|^2$, all colors) and of the confined light mode ($|\alpha^K|^2$, grey) of the polaritonic state (K) on which the 101-molecule trajectory evolves. Bottom left: populations of the 102 polaritonic states ($c(t)_K^* c(t)_K$, equation 9). State of lowest energy ($K = 0$) in black, second-lowest ($K = 1$) in red, third-lowest ($K = 2$) in green, etc. Bottom right: hopping probabilities (equation 13) for transition from state 0 into state 1 (black) and back (red). Surface hops from state 0 to 1 are indicated by black dashed lines, hops from 1 to 0 as red dashed lines.

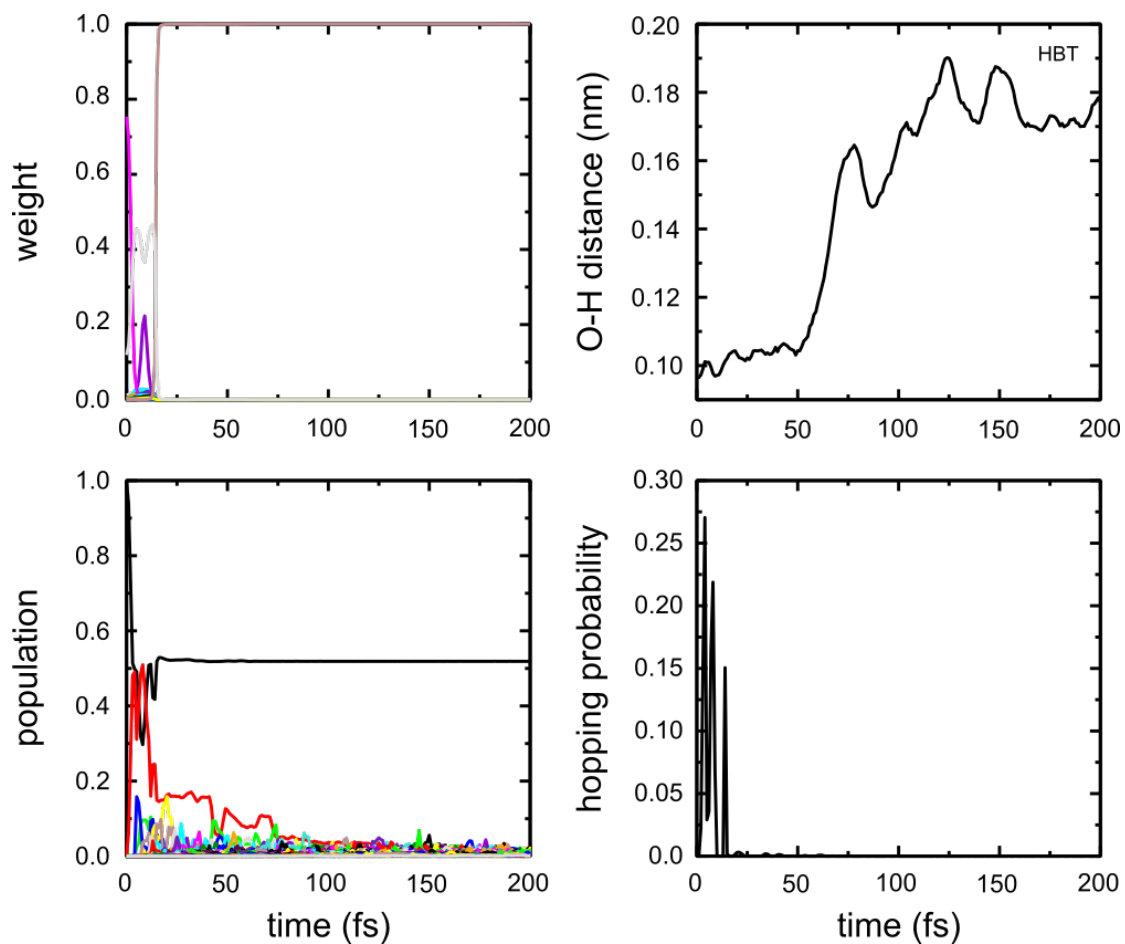


Figure S29: Time-evolution of the polaritonic state and the O-H distance (top right) in HBT during 200 fs of FSSH MD simulation with 100 Rhodamines and 1 HBT molecule (plus environment) strongly coupled to confined light (simulation 12, Table S2). Top left: weights of the excitations on each molecule ($|\beta_i^K|^2$, all colors) and of the confined light mode ($|\alpha^K|^2$, grey) of the polaritonic state (K) on which the 101-molecule trajectory evolves. Bottom left: populations of the 102 polaritonic states ($c(t)_K^* c(t)_K$, equation 9). State of lowest energy ($K = 0$) in black, second-lowest ($K = 1$) in red, third-lowest ($K = 2$) in green, etc. Bottom right: hopping probabilities (equation 13) for transition from state 0 into state 1 (black).

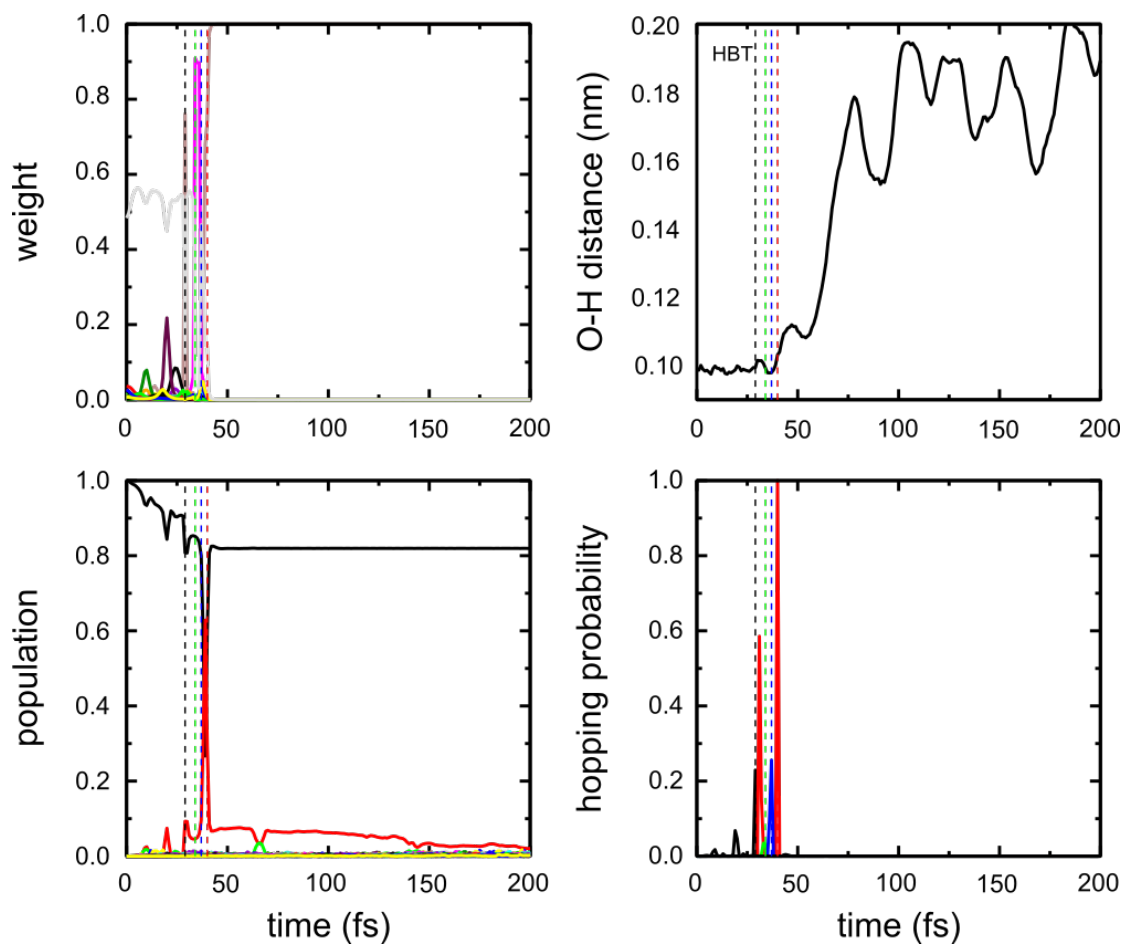


Figure S30: Time-evolution of the polaritonic state and the O-H distance (top right) in HBT during 200 fs of FSSH MD simulation with 100 Rhodamines and 1 HBT molecule (plus environment) strongly coupled to confined light (simulation 13, Table S2). Top left: weights of the excitations on each molecule ($|\beta_i^K|^2$, all colors) and of the confined light mode ($|\alpha^K|^2$, grey) of the polaritonic state (K) on which the 101-molecule trajectory evolves. Bottom left: populations of the 102 polaritonic states ($c(t)_K^* c(t)_K$, equation 9). State of lowest energy ($K = 0$) in black, second-lowest ($K = 1$) in red, third-lowest ($K = 2$) in green, etc. Bottom right: hopping probabilities (equation 13) for transition from state 0 into state 1 (black) and back (red). Surface hops from state 0 to 1 are indicated by black dashed lines, hops from 1 to 0 as red dashed lines, hops from 1 to 2 as green dashed lines and hops from 2 to 1 as blue dashed lines.

Animations

QuickTime animations of excited state intramolecular proton transfer in an isolated HBT molecule (HBT.qt) and in an HBT molecule inside a cavity with 5 HBT and 500 Rho molecules (HBTcav.qt) are available for download from pubs.acs.org. In these movies, a flash illustrates the instantaneous photon absorption. The carbon atoms in the chromophore are colored green in the ground state (S_0) and cyan in the excited state (S_1). The snapshots for these animations were created with Molscrip⁴¹ in combination with Raster3D.⁴²

References

1. Luk, H. L.; Feist, J.; Toppari, J. J.; Groenhof, G. Multi-scale molecular dynamics simulations of polaritonic chemistry. *J. Chem. Theory Comput.* **2017**, *13*, 4324-4335.
2. Jaynes, E. T.; Cummings, F. W. Comparison of quantum and semiclassical radiation theories with application to the beam maser. *Proc. IEEE*, **1963**, *51*, 89-109.
3. Tavis, M.; Cummings, F. W.; Exact solution for an N-molecule-radiation-field Hamiltonian. *Phys. Rev.* **1969**, *188*, 692-695.
4. Galego, J.; Garcia-Vidal, F. J.; Feist, J. Cavity-induced modifications of molecular structure in the strong coupling limit. *Phys. Rev. X* **2015**, *5*, 041022.
5. DeLiberato, S. Light-Matter Decoupling in the Deep Strong Coupling Regime: The Breakdown of the Purcell Effect. *Phys. Rev. Lett.* **2014**, *112*, 016401
6. Flick, J.; Ruggenthaler, M.; Appel, H.; Rubio, A. Cavity Born–Oppenheimer Approximation for Correlated Electron–Nuclear–Photon Systems. *J. Chem. Theory Comput.* **2017**, *13*, 1616–1625.
7. Flick, J.; Ruggenthaler, M.; Appel, H.; Rubio, A. Atoms and molecules in cavities, from weak to strong coupling in quantum-electrodynamics (QED) chemistry. *Proc. Natl. Acad. Sci. USA*, **2017**, *114*, 3026–3034.
8. Boggio-Pasqua, M.; Burmeister, C. F.; Robb, M. A.; Groenhof G. Photochemical reactions in biological systems: probing the effect of the environment by means of hybrid quantum chemistry/molecular mechanics simulations. *Phys. Chem. Chem. Phys.* **2012**, *14*, 7912 – 7928.
9. Tully, J. C. Molecular dynamics with electronic transitions. *J. Chem. Phys.* **1990**, *93*, 1061.
10. Landau, L. Zur Theorie der Energieübertragung II. *Phys. Z. Sowjetunion* **1932**, *2*, 1–13.
11. Zener, C. Non-adiabatic crossing of energy levels. *Proc. R. Soc. A* **1932**, *137*, 696–702.
12. Desouter-Lecomte, M.; Lorquet, J. Nonadiabatic interactions in unimolecular decay. IV. Transition probability as a function of the Massey parameter. *J. Chem. Phys.* **1979**, *71*, 4391–4403.
13. Hammes-Schiffer, S.; Tully, J. C. Proton transfer in solution: molecular dynamics with quantum transitions. *J. Chem. Phys.* 1994, *101*, 4657–4667
14. Fabiano, E.; Groenhof, G.; Thiel, W. Approximate switching Algorithms for Trajectory Surface Hopping. *Chem. Phys.* **2008**, *351*, 111–116.

15. Wang, L.; Prezhdo, O. V. A Simple Solution to the Trivial Crossing Problem in Surface Hopping. *J. Phys. Chem. Lett.* **2014**, *5*, 712–119.
16. Hess, B.; Kutzner, C.; van der Spoel, D.; Lindahl, E. GROMACS 4: Algorithms for Highly Efficient, Load-Balanced, and Scalable Molecular Simulation. *J. Chem. Theory Comput.* **2008**, *4*, 435–447.
17. Duan, Y.; Wu, C.; Chowdhury, S.; Lee, M. C.; Xiong, G. M.; Zhang, W.; Yang, R.; Cieplak, P.; Luo, R.; Lee, T.; Caldwell, J.; Wang, J. M.; Kollman, P. A point-charge force field for molecular mechanics simulations of proteins based on condensed-phase quantum mechanical calculations. *J. Comput. Chem.* **2003**, *24*, 1999–2012.
18. Horta, B. A. C.; Merz, P. T.; Fuchs, P. F. J.; Dolenc, J.; Riniker, S.; Hünenberger, P. H. A GROMOS-Compatible Force Field for Small Organic Molecules in the Condensed Phase: The 2016H66 Parameter Set. *J. Chem. Theory Comput.* **2016**, *12*, 3825–3850.
19. Jorgensen, W. L.; Chandrasekhar, J.; Madura, J. D.; Impey, R. W.; Klein, M. L. Comparison of simple potential functions for simulating liquid water. *J. Chem. Phys.* **1983**, *79*, 926–935.
20. Berendsen, H.; Postma, J.; van Gunsteren, W.; Ja, A. D.; Haak, J. Molecular dynamics with coupling to an external bath. *J. Chem. Phys.* **1984**, *81*, 3684–3690.
21. Hess, B.; Bekker, H.; Berendsen, H. J. C.; Fraaije, J. G. E. M. LINCS: A linear constraint solver for molecular simulations. *J. Comput. Chem.* **1997**, *18*, 1463–1472.
22. Miyamoto, S.; Kollman, P. A. SETTLE: An analytical version of the SHAKE and RATTLE algorithms for rigid water molecules. *J. Comp. Chem.* **1992**, *18*, 1463–1472.
23. Essmann, U.; Perera, L.; Berkowitz, M. L.; Darden, T.; Lee, H.; Pedersen, L. G. A smooth particle mesh Ewald potential. *J. Chem. Phys.* **1995**, *103*, 8577–8592.
24. Becke, A. D. A new mixing of Hartree-Fock and local density-functional theories. *J. Chem. Phys.* **1993**, *98*, 1372.
25. Lee, C. T.; Yang, W. T.; Parr, R. G. Development of the Colle-Salvetti correlation-energy formula into a functional of the electron density. *Phys. Rev. B* **1988**, *37*, 785–789.
26. Yanai, T.; Tew, D. P.; Handy, N. C. A new hybrid exchange-correlation functional using the Coulomb-attenuating method (CAM-B3LYP). *Chem. Phys. Lett.* **2004**, *393*, 51–57.
27. Dunning, T. H. Gaussian Basis Functions for Use in Molecular Calculations. I. Contractions of (9s5p) Atomic Basis Sets for the First-Row Atoms. *J. Chem. Phys.* **1970**, *53*, 2823–2833.
28. Runge, E.; Gross, E. K. U. Density-Functional Theory for Time-Dependent Systems. *Phys. Rev. Lett.* **1984**, *52*, 997–1000.
29. Barbatti, M.; Aquino, A. J. A.; Lischka, H.; Schriever, C.; Lochbrunner, S.; Riedle, E. Ultrafast internal conversion pathway and mechanism in 2-(2'-hydroxyphenyl)benzothiazole: a case study for excited-state intramolecular proton transfer systems. *Phys. Chem. Chem. Phys.*, **2009**, *11*, 1406–1415.
30. Pijeu, S.; Foster, D.; Hohenstein, E. G. Excited-state dynamics of 2-(2'-hydroxyphenyl) benzothiazole: ultrafast proton transfer and internal conversion. *J. Phys. Chem. A* **2017**, *121*, 4595–4605.

31. Lochbrunner, S.; Wurzer, A. J.; Riedle, E. Microscopic mechanism of ultrafast excited-state intramolecular proton transfer: a 30-fs study of 2-(2'-hydroxyphenyl) bezothiazole. *J. Phys. Chem. A* **2003**, *107*, 10580-10590.
32. George, J.; Wang, S.; Chevry, T.; Canaguier-Durand, A.; Schaeffer, G.; Lehn, J.-M.; Hutchison, J. A.; Genet, C.; Ebbesen, T. W. Ultra-strong coupling of molecular materials: spectroscopy and dynamics. *Faraday Discuss.* **2015**, *178*, 281-294.
33. Schwartz, T.; Hutchison, J. A.; Leonard, J.; Genet, C.; Haacke, S.; Ebbesen, T.W. Polariton Dynamics under Strong Light-Molecule Coupling. *ChemPhysChem* **2013**, *14*, 125–131.
34. Zengin, G.; Wersäll, M.; Nilsson, S.; Antosiewicz, T. J.; Käll, M.; Shegai, T. Realizing strong light-matter interactions between single-nanoparticle plasmons and molecular excitations at ambient conditions. *Phys. Rev. Lett.* **2015**, *114*, 157401.
35. Melnikau, D.; Esteban, R.; Savateeva, D.; Sánchez-Iglesias, A.; Grzelczak, M.; Schmidt, M. K.; Liz-Marzán, L. M.; Aizpurua, J.; Rakovich, Y. P. Rabi Splitting in Photoluminescence Spectra of Hybrid Systems of Gold Nanorods and J-Aggregates. *J. Phys. Chem. Lett.* **2016**, *7*, 354–362.
36. Lindblad, G. On the generators of quantum dynamical semigroups. *Comm. Math. Phys.* **1976**, *48*, 119–130.
37. Frisch, M. J.; Trucks, G. W.; Schlegel, H. B.; Scuseria, G. E.; Robb, M. A.; Cheeseman, J. R.; Scalmani, G.; Barone, V.; Mennucci, B.; Petersson, G. A.; Nakatsuji, H.; Caricato, M.; Li, X.; Hratchian, H. P.; Izmaylov, A. F.; Bloino, J.; Zheng, G.; Sonnenberg, J. L.; Hada, M.; Ehara, M.; Toyota, K.; Fukuda, R.; Hasegawa, J.; Ishida, M.; Nakajima, T.; Honda, Y.; Kitao, O.; Nakai, H.; Vreven, T.; Montgomery, J. A., Jr.; Peralta, J. E.; Ogliaro, F.; Bearpark, M.; J. Heyd, J.; Broth-ers, E.; Kudin, K. N.; Staroverov, V. N.; Kobayashi, R.; Normand, J.; Raghavachari, K.; Rendell, A.; Burant, J. C.; Iyengar, S. S.; Tomasi, J.; Cossi, M.; Rega, N.; Millam, J. M.; Klene, M.; Knox, J. E.; Cross, J. B.; Bakken, V.; Adamo, C.; Jaramillo, J.; Gomperts, R.; Stratmann, R. E.; Yazyev, O.; Austin, A. J.; Cammi, R.; Pomelli, C.; Ochterski, J. W.; Martin, R. L.; Morokuma, K.; Zakrzewski, V. G.; Voth, G. A.; Salvador, P.; Dannenberg, J. J.; Dapprich, S.; Daniels, A. D.; Farkas, Ö.; Foresman, J. B.; Ortiz, J. V.; Cioslowski, J.; Fox, D. J. Gaussian 09 Revision D.1. Gaussian Inc. Wallingford CT 2009.
38. Lee, J.; Kim, C. H.; Joo, T. Active Role of Proton in Excited State Intramolecular Proton Transfer Reaction. *J. Phys. Chem. A*, **2013**, *117*, 1400–1405.
39. O. Vendrell, Collective Conical Intersections through Light-Matter Coupling in a Cavity, [arXiv:1806.07252v1](https://arxiv.org/abs/1806.07252v1) [[physics.chem-ph](https://arxiv.org/archive/physics)]
40. Barbatti, M. Nonadiabatic dynamics with trajectory surface hopping method, *WIREs Comp. Mol. Sci.*, **2011**, *1*, 620–633.
41. Kraulis, P. J. MOLSCRIPT: a program to produce both detailed and schematic plots of protein structures. *J. Appl. Crystallogr.*, **1991**, *24*, 946-950.
42. Merrit, E. A.; Bacon, D. J. Raster3D: photorealistic molecular graphics. *Meth. Enzymol.*, **1997**, *277*, 505-524.